Studies of Novel Small Molecule and Polymer blends for Application in Organic Light-Emitting Diodes

Thesis by

Despoina Gkeka

In Partial Fulfillment of the Requirements

For the Degree of

Master of Science

King Abdullah University of Science and Technology

Thuwal, Kingdom of Saudi Arabia

April,2021

EXAMINATION COMMITTEE PAGE

The thesis of Despoina Gkeka is approved by the examination committee.

Committee Chairperson: Prof. Thomas Anthopoulos
Committee Members: Prof. Thomas Anthopoulos, Prof. Frederic Laquai, Prof. Iain McCulloch, Prof. Vincent Tung

ABSTRACT

Studies of Novel Small Molecule and Polymer blends for Application in Organic Light-Emitting Diodes

Despoina Gkeka

Display technology has become a vital and ubiquitous part of our daily life. Undoubtedly, today's technologically minded society is living in the era of the digital image. After high resolution and efficiency could successfully be realized, the major trends in display technology now aim towards achieving high color purity for natural looking display colors. Organic light-emitting diodes (OLEDs), as one strong contender for high performance displays and lighting, have been undergoing tremendous industrial and commercial development. Despite the great progress, though, there is still space for improvement, especially in the case of blue light emitting devices. Blue OLEDs are always challenging, since they traditionally suffer from low efficiencies and lifetimes. Both, novel materials and device architectures, are driving ongoing developments while still always aiming to lower the overall costs. In a continual effort to search for robust materials for blue devices, small molecules (SMs) and polymers, are shown to be promising candidates. In this thesis is presented the results of the detailed study of photophysical and electroluminescence (EL) properties in the case of thin films based on blends of the conjugated polymer Poly(9,9-di-n-octylfluorenyl-2,7-diyl) (PFO) and the of novel SMs; 4,4'-(anthracene-9,10-diyl)bis(N,N-bis(4-methoxyphenyl)aniline) (TPAA) and 4,4'-

(pyrene-1,6-diyl)bis(N,N-bis(4-methoxyphenyl)aniline) (TPAP). Finally, devices based on these systems are optimized step by step as a solution processable emissive layer (EML), for applications in sky blue OLEDs.

ACKNOWLEDGEMENTS

There are several people who deserve my honest thank you. Accept my kind apologies in case I forget to include you in my list. Firstly, I would like to thank my Advisor, Prof. T. Anthopoulos, for his guidance and support throughout the course of this research. A great thank you to M. Neophytou, who firstly introduced me to the fascinating field of LEDs and for the Hyperspectral measurements. Also to R. Hallani for the synthesis of the small molecules, professor L. Tsetseris for DFT and A. Seitkahn for TEM measurements. Lastly, E. Yengel and J. Khan for Impedance and Transient-PL measurements respectively. It would have been impossible to fulfill this research without your experience and help.

My appreciation also goes to my friends and colleagues of LAMA group at King Abdullah University of Science and Technology. Finally, my heartfelt gratitude is extended to family and friends for their encouragement and especially to Mihalis for his patience and support.

"As we work to create light for other, we naturally light our own way"

M.A.Radmacher

Table of Contents

LIST OF ABBREVIATIONS

A Anode

AFM Atomic Force Microscopy

BCP Bathocuproine

CIE Commission Internationale de l'Eclairage

DFT Density Functional Theory

DI De-Ionized Water

EA Electron Affinity

EL Electroluminescence

EML Emissive Layer

EQE External Quantum Efficiency

ETL Electron Transport Layer

FRET Förster resonant energy transfer

HLM Hyperspectral Luminescence Microscopy

HOMO Highest Occupied Molecular Orbital

HTL Hole Transport Layer

IP Ionization Potential

IQE Internal Quantum Efficiency

IS Impedance Spectroscopy

ITO Indium Tin Oxide

K Cathode

LUMO Lowest Unoccupied Molecular Orbital

OLEDs Organic Light-Emitting Diodes

PEDOT:PSS P(3,4-ethylenedioxythiophene):poly(4 styrenesulfonate)

PESA Photoelectron Spectroscopy in Air

PFO	Poly(9,9-di-n-octylfluorenyl-2,7-diyl)
PL	Photoluminescence
rpm	Revolutions Per Minute
SAM	Self-Assembled Monolayer
SMs	Small Molecules
TADF	Thermally Activated Delayed Fluorescence
TEM	Transmission Electron Microscopy
TPAA	4,4'-(anthracene-9,10-diyl)bis(N,N-bis(4-methoxyphenyl)aniline)
TPAP	4,4'-(pyrene-1,6-diyl)bis(N,N-bis(4-methoxyphenyl)aniline)
3D	Three Dimensional
2D	Two Dimensional
TR-PL	Time Resolved Photoluminescence
UV	Ultraviolet

LIST OF SYMBOLS

λ	indicates the wavelength of electromagnetic radiation
S_o	refers to the ground state
S_1	refers to higher (excited) energy states
n_{ext}	refers to external quantum efficiency
n_{int}	refers to internal quantum efficiency
n_{inj}	refers to injection efficiency
n_{extr}	refers to light extraction efficiency
S	is the spin quantum number
Eg	refers to the Energy Band Gap
h	is Planck's constant
c	is the speed of Light
Å	Angstrom (units)
Ag	Silver
J	Current Density
I	Current
R	Resistance
C	Capacitance
Z	Impedance
w	is the angular frequency
ps	refers to picosecond

LIST OF ILLUSTRATIONS

LIST OF TABLES

Chapter 1

1.1 Introduction

Since 1987 when Tang et al. [8] demonstrated the successful interpretation of OLEDs based on SMs, OLEDs have attracted wide attention for their great potential in flat-panel displays and solid state lighting. Shortly afterwards, Burroughes et al. [9] demonstrated conjugated polymers as another reliable candidate for OLEDs. These are the major discoveries which introduced OLEDs as a promising display technology and essentially revolutionized the field, allowing for new applications of higher quality and possibilities. They offer a plethora of attractive characteristics, especially compared due inorganic LEDs, such as low-cost synthesis and simple manufacturing process (solution processing). In addition, they offer high resolution, high speed and good color purity [3]. Due to their outstanding characteristics, OLEDs are nowadays already well-established in the market.

Regardless of the aforementioned progress and historically speaking, efficient blue LEDs (organic or inorganic) has always been more demanding [10]–[13]. It is worth mentioning that Isamu Akasaki, Hiroshi Amano and Shuji Nakamura won the 2014 Nobel Prize in Physics for their contribution to efficient blue GaN LEDs [14]. Typically, efficient and stable blue light emitting diodes are more challenging compared to their green or red counterparts [15]. Blue emitters are materials with a large band gap, which can give rise to several non-radiative effects, resulting in reduced device performance [12], [13]. Therefore, further research is still needed in order to fulfill the requirements for all

practical applications, including even higher efficiencies and stability (see Figure 1.1), while keeping the cost relatively low.

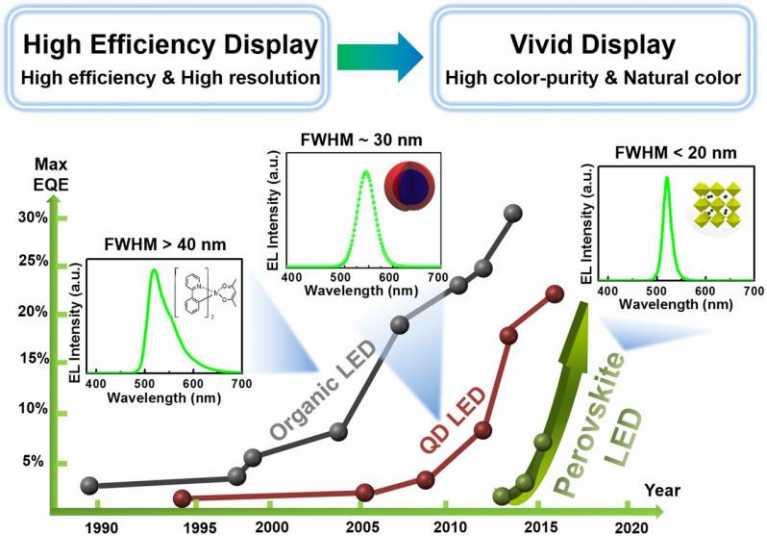

Figure 1.1 Major trend of display technology. Starting from Organic LED (1990), the trend moved towards Quantum Dots LEDs (until 2015) and afterwards Perovskite LEDs (2015-). However Organic LEDs still remain the most efficient display [10].

Chapter 2: Theoretical Background

2.1 Fundamentals: Luminescence

The term luminescence was firstly introduced by a German physicist named Eilhard Wiedemann and its origin is Latin, “Lumen”, which means light. Luminescence is used to describe the principles of absorption and emission of radiation (light) by matter. The materials which are capable of luminescence emission are called luminophors or phosphors. The luminescence process as it shown in Figure 2.1, is cold emission (no heat production) generated due to the transitions of electrons from higher energetic states to lower energetic states [16].

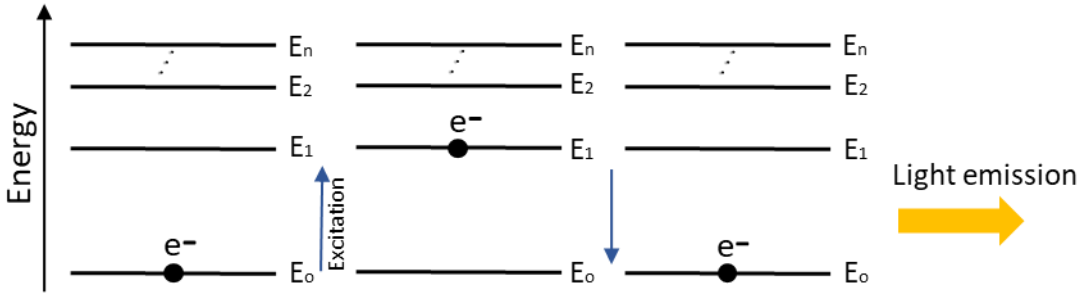

Figure 2.1: Representation of the luminescence process in a system with n number of energy states: Initially the electron is in the ground state (E_o), during excitation electron is promoted to higher energy states (E_1). Finally electron returns to ground state and light emission occurs.

Based on the luminescence law, the wavelength (λ) of the emitted radiation is always greater compared to the wavelength of the exciting radiation ($\lambda_{emi} > \lambda_{exc}$). Moreover, the wavelength of the light which is emitted essentially characterizes the luminescent material or substance [3].

Various categories of luminescence [17], [18] exist in nature, depending on the process that generates the excited electron(s):

- Photoluminescence
- Electroluminescence (EL)
- Biochemical-luminescence
- Mechanoluminescence
- Thermoluminescence

2.2 Basic Principles of OLEDs

2.2.1 OLED Structure

Fundamentally in an OLED device the different organic (and/or inorganic) layers are "sandwiched" between the two electrodes, the anode and the cathode. In Figure 2.2 is shown a typical multilayered OLED device.

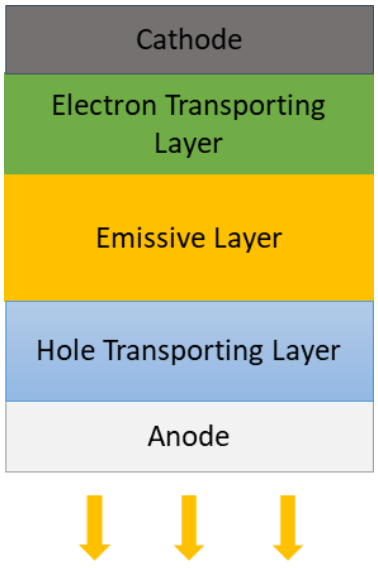

Figure 2.2: Typical device configuration of an organic light emitting diode. The active layers sandwiched between the anode and the cathode and light emission through the transparent electrode and substrate.

The basic layers of an OLED device and the functions of each (see Figure 2.3), are described as:

- Anode (A): Injects holes into the hole transport layer (HTL). It is a transparent material, most commonly Indium Tin Oxide (ITO), which enables the transmission of the emitted light out of the device.
- Hole transport layer (HTL): Supports the transference of holes towards emission layers and additionally, opposes electron transfer from the cathode toward the anodes.
- Emission layer (EML): It is the main component of an OLED and essentially is the layer in which photons are generated. Allows hole and electron injection from adjoining layers by suitable highest occupied molecular orbital (HOMO) and lowest unoccupied molecular orbital (LUMO) positions of the emission layer and is the layer in which photons are generated.
- Electron transport layer (ETL): Complementary to hole transport layer, it promotes the transport of electrons towards the emission layer.
- Cathode (K): Injects electrons into the ETL. Typically it corresponds to a low work function material [19].

Essentially, an OLED utilizes the principle of EL. Under bias application to the device, charge carriers are injected from the electrodes to the organic layers. Holes (positive charge) are injected from the anode and electrons (negative charge) are injected from the

cathode. The holes and electrons are transported to the EML and eventually excitons are formed. Finally, due to radiative relaxation of the excitons, photons are generated resulting in light emission. [20]. The wavelength of this light emission resembles to the exciton energy (excitons will be further discussed in 2.4.1 section). Therefore, it is possible to manipulate the color of the light emission simply via applying molecular design strategies to the emissive layer [19].

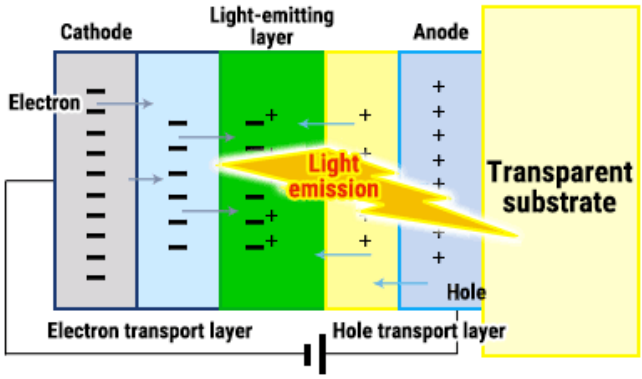

Figure 2.3: Light emission mechanism of organic light emitting diodes. The mechanism is based on the electroluminescence process in which the organic light-emitting layer emits light in a response to applied electric field [21].

2.2.2 Deposition Techniques for OLED Fabrication

Deposition techniques related to the fabrication of OLEDs can be classified into two main categories, which are either solution based or dry techniques. While choosing the kind of deposition, the chemistry of the respective material that is going to be deposited must be considered. Of course other parameters, such as the cost and ease of reproducibility, also play a key role. For example, in the case of polymer organic materials, solution based can be adopted. This category includes methods such as spin-coating and ink jet printing etc.

Typical dry techniques on the other hand include vacuum thermal evaporation and organic vapor phase deposition. These techniques are primarily used for the deposition of small molecular organic system and allow the convenient deposition of uniform and homogenous films. It is also possible to process SMs with solution based techniques, however, small aromatic molecules tend to be less soluble (compared to polymers), making it more challenging to deposit sufficiently thick films. In the next paragraphs, two of the main deposition methods that were also used in the current thesis, are explained in more detail.

Spin-coating

Spin- coating is one of the most commonly used deposition techniques. As can be seen in Figure 2.4, it is quite straightforward and fast. During this process, a quantity of a solution, often consisting of a polymer dissolved into an organic solvent, is deposited onto a substrate while using spinning until it dries, typically of speed range between 1000-10000 revolutions per minute (rpm). Notably, the effect of centrifugal force during spinning, results in expel of great amount of the solution. Nevertheless, part of the solution is left behind, allowing the coating of the whole substrate. Generally, the precise thickness of the final film is quite difficult to predict [22], [23].

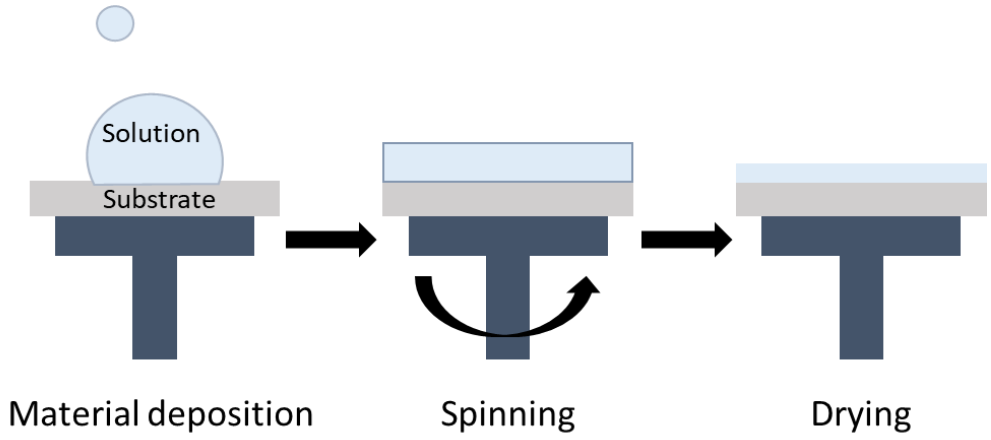

Figure 2.4: Stages of a typical spin-coating deposition process. In the first step, the material is deposited in the form of solution, followed by the stage of spinning. Finally, throughout the process, drying of the solution occurs.

Vacuum Thermal Evaporation

During vacuum deposition, a boat made out of alumina or a metal (such as tungsten, molybdenum etc.) is heated using electric current. The material is inserted to the boat and upon heating, evaporates or sublimes. A typical vacuum thermal evaporation system is shown in Figure 2.5. The evaporation process is carried out low pressure vacuum chamber, typically under 10^{-6} Torr. In this way, deposited materials are kept pure and also the probability on evaporated material to experience possible collisions is minimized. Every molecule that released from the solid has an initial speed and direction which remain unchanged until it meets the substrate surface and condensates [24], [25]. Materials are patterned using shadow masking in order to control the areas in which deposition takes place [24].

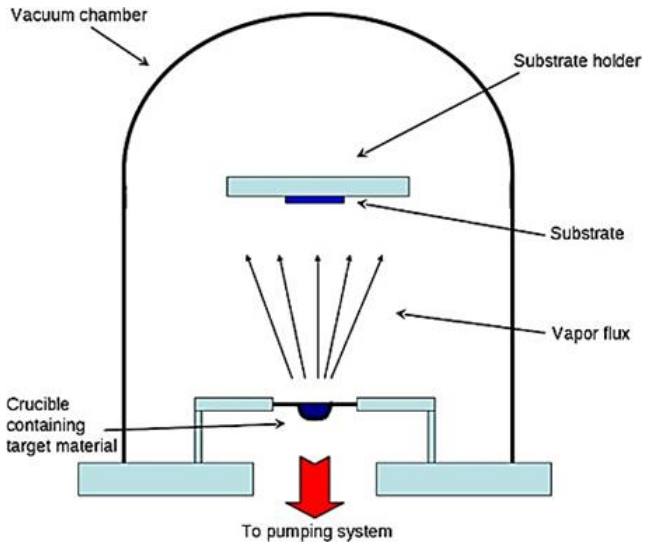

Figure 2.5: Schematic of a vacuum thermal evaporation system [25].

2.3 Working Principles of OLEDs

There are three stages, related to the working mechanism of an OLED, which are extremely vital. Carrier injection, carrier transport and carrier recombination and emission [26], [27].

2.3.1 Carrier Injection

During this stage and under forward bias application, holes are injected from the anode into the HTL and electrons are injected from the cathode into the ETL. Carrier injection has a great impact in the optimization of the device efficiency, considering that it affects electron/hole balance in the device and hence, the exciton distribution [28], [29].

2.3.2 Carrier Transport

Organic semiconductors often exhibit a great amount of structural disorder compared to inorganic semiconductors, causing the disappearance of a continuous band found for the

single crystal structures of inorganic semiconductors. Instead, many individual HOMO and LUMO states localized on individual molecules appear. The distribution of these states with respect to the energy can be described by a Gaussian distribution. Clearly, any charge transport happens between localized states and, therefore, the charge carriers have to overcome the potential barrier resulting from the localization. In addition, curves and twists of the polymer backbone, as well as impurities incorporated during the synthesis further lower the observed charge carrier mobilities (from 10^{-5} cm²/ V·s to 10^{-1} cm²/ V·s). As a consequence, the charge carriers are not able to move freely through the material and the transport can be described by a thermally activated (phonon assisted) hopping process from one state localized at one molecule to the next state localized at a neighboring one.

In an OLED device, the transport of carriers across the thin organic is fulfilled through the hopping process of carriers, under the effect of an applied bias. The existence of traps in the organic layers is very important and essentially divides charge transport into four different regimes: ohmic, space-charge limited, trap-charge limited and trap-filled [26], [27].

i. *Ohmic transport regime*: Under the application of a very low electric field, charge transport is limited only by the contact interface between the electrodes and the organic layers. The bulk of the organics is not considered. Therefore, typically, ohmic behavior is exhibited by the charge (electron and holes) currents.

ii. *Space-charge limited transport regime*: Further increase of the bias, generates a space charge at the interface. As a result, carrier injection is also increased. Under

increased applied voltage, charge accumulation in the organic layer is facilitated, due to strong carrier injection into the low-mobility materials. This charge build-up strikes partially the applied field. As a result, it is re-arranged and the I-V characteristics behavior is justified as space-charge limited regime.

iii. *Trap-charge limited transport regime*: In the case that high electric field, an enormous number of carriers is injected into the organic layers. Hence, the traps that might exist, are filled up. This results in the so called trap-charge limited regime.

iv. *Trap filled space-charge limited transport regime*: When additional injected carriers and all the trap sites are occupied, electrons and holes can move freely in the presence of space-charge effects, only without any influence of charge trapping. This is considered as the trap-filled space-charge limited transport regime [26]–[29].

2.3.3 Carrier Recombination and Emission

As already mentioned, electrons and holes are transported from the electrodes across the organic layers and eventually experience a coulombic interaction. As a result, the so called exciton is formed and energy as a photon is released (light). As will be discussed further in following sections, the exciton's nature is extremely important. It characterizes the material itself but also sets limits to OLEDs efficiencies [27], [29].

2.4 Organic Semiconductors

2.4.1 Excitons

Organic semiconductors are carbon-based materials which demonstrate semiconducting properties [1]. Most of the optical and optoelectronic properties of these materials are predominantly determined by excitons. Essentially, an exciton corresponds to a bound pair of an electron and a hole which experience a Coulombic interaction [30]. In the case of organic semiconductors, the term exciton refers to molecular excited states which are generated inside the solid and can be transferred. The excitonic phenomena arise from the relatively weak van der Waals forces, which bound the material in the solid state. This comes into contradiction with the case of inorganic semiconductors which are strongly bound by ionic/ covalent bonds. In this case, crystal lattice is formed through electron sharing by all the ions. Consequently, in organic semiconductors the excitons are strongly bound into small Frenkel-like states, whilst in the inorganics, excitons are lightly bound Wannier–Mott states and can be unstable at room temperature [31].

2.4.2 Singlet and Triplet States

As already mentioned, the excitonic nature defines the type of a material. There are two categories which are possible to occur, depending on the spin configuration. In singlet excitons, the spin of the LUMO electron can pair with that of the HOMO electron (see Figure 2.6). Hence, singlets are states with an antisymmetric spin and a total spin quantum number $S = 0$.

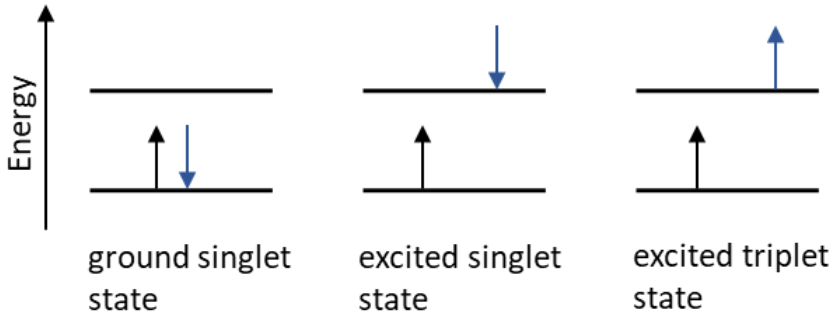

Figure 2.6: Schematic diagram of singlet and triplet states configuration.

In the case of the so called triplet excitons, the spin of the LUMO electron does not pair with that of the HOMO electron. Therefore, triplet excitons encounter symmetric spin configuration of S= 1. The existence of singlet and/or triplet states characterize the type of the emitting material. As will be further explained in the next section, sets up important limitations to the theoretical efficiency of an OLED device.

2.5 Characteristic Performance Parameters of OLEDs

It is fundamental to quantify and investigate the factors which can affect the performance of and OLED device. The external quantum efficiency (EQE or n_{ext}) and internal quantum efficiency (IQE) are some of the most common indicators of how effectively an OLED device is emitting light. External quantum efficiency essentially represents the number of photons emitted externally from the LED device per injected electrons. EQE equation for OLEDs is given [13],[27]:

$$EQE = \gamma \times n_s \times \Phi_f \times n_{extr} \qquad \text{(Eq. 2.1)}$$

Analyzing further each component of the previous equation:

- γ is called charge balance factor and corresponds to the number of injected charges that generates excitons.
- n_s is the singlet exciton efficiency and refers to the fraction of singlet excitons
- Φ_f is called quantum efficiency of fluorescence and corresponds to the fraction of energy released from the material as photons (light).
- Light extraction efficiency (n_{extr}) is the number of photons emitted out of the LED to the total number of produced photons.

IQE is described as the ratio of the number of photons produced within the OLED device per injected electrons [32]. IQE is given by the following equation:

$$IQE = \gamma \times n_s \times \Phi_f \quad \text{(Eq. 2.2)}$$

As will be discussed in the following section, fluorescent materials are unable to harness triplet excitons. Consequently, fluorescent materials can only theoretically achieve 25% internal quantum efficiency (IQE). This limited theoretical value comes to disagreement with the requirements of commercial applications.

2.6 Energy Transfer

2.6.1 Intramolecular Energy Transfer

The processes of a molecular system which occur due to electronic transitions, are usually illustrated by Jablonski diagram. A typical Jablonski diagram is shown in Figure 2.7. The excited species release energy through several mechanisms, namely vibrational

relaxation, internal conversion, intersystem crossing, fluorescence and phosphorescence [18], [33].

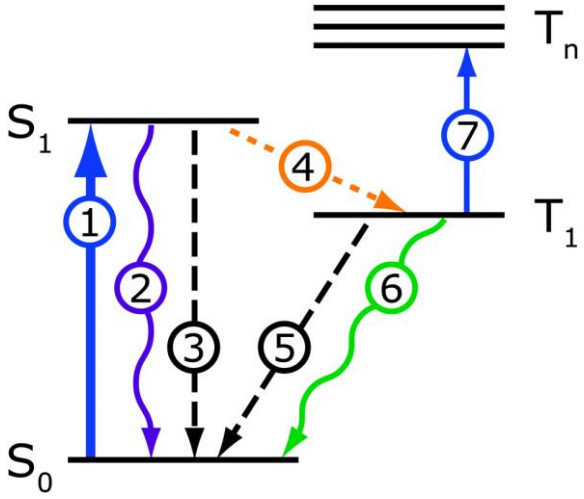

Figure 2.7: Electronic transitions found in Organic Semiconductors, presented as arrows: (1) Absorption, (2) Fluorescence, (4) Intersystem crossing, (6) Phosphorescence, (3 and 5) Non-radiative, and (7) Photo-induced Absorption. The energies of singlet (S_0 and S_1) and triplet (T_1 and T_n) states are scaled vertically [1].

Absorption: Among the various transitions, absorption is the fastest, occurring in roughly 10^{-15} s. Absorption process is illustrated on the Jablonski diagram as $S_0 \rightarrow S_1$ transition. It arises from excitation by species with energies higher than that of the bandgap energy Eg = hc/λ, where h is Planck's constant, c is the speed of light, and λ is the wavelength of a photon emitted upon decay from the lowest excited state to the ground state. Since absorption is possible to occur over a range of energies, its spectrum consists of a broad peak [33]–[35].

Fluorescence: In general, fluorescence is a property of particular substances (atoms or molecules) to absorb light of specific wavelength, followed by light emission of longer wavelength. Light emission occurs after a short delay which corresponds to the lifetime

of fluorescence [1], [16]. As an example, consider a system in which some atoms exist in the ground state (S_o). If these atoms are exposed to visible or ultraviolet (UV) radiation, they absorb energy as photons and occupy higher energy states (S_1). These energy states are identified as excited singlet states, with lifetimes of about 10^{-8} s. Eventually, the extra energy of the excited electrons is released as photons, resulting in a transition back to the ground state (singlet state). During this process excitation energy is emitted as fluorescence [1]. Fluorescence is a very fast process. Throughout this effect, the spin of the electron remains the same. The singlet ground state and the excited singlet state have same multiplicity, ending within about 10^{-8} s after excitation [3]. Many processes can affect the intensity of fluorescence, such as quenching which can result in decreased intensity of fluorescence. Quenching can occur by different mechanisms and includes energy transfer, collisional quenching and excited state reactions. Materials that exhibit fluorescent emission, are fundamentally incapable to make use of the triplet excitons. However, triplet excitons represent three quarters of all electrically generated excitons. Thus, severe efficiency limitations are present in fluorescent materials. Consequently, fluorescence can theoretically only achieve 25% IQE, lacking the skill to meet the expectations of commercial applications [36].

Intersystem Crossing: Typically, transitions between a singlet state and a triplet state, or between a triplet state and ground state, quantum mechanically forbidden. However, it is possible to occur through a mechanism called intersystem crossing (ISC), which involves a spin change [37]. This does not occur unless there is some degree of spin-orbit

interaction, denoted spin-orbit coupling (SOC) [34], [35]. ISC is fundamental for the excited state decay dynamics of several molecular systems and is very characteristic of systems which contain heavy elements, such as Iridium.

Phosphorescence: In contrast with fluorescent materials, a phosphorescent material does releases gradually, in the form of photons (light), the energy (radiation) it absorbs. This results in a more delayed luminescence compared to the fluorescence process. In phosphorescence an electron can be promoted to a higher energy level, which is called excited triplet state. Finally, relaxation back to ground singlet state, accompanied by light emission occurs. However, the lifetime of triplet states is substantially longer compared to the singlet states. The lifetime of an excited triplet state can be up to 10 seconds, in comparison with the 10^{-5} to 10^{-8} s average lifetime of an excited singlet state. Phosphorescent materials are capable of taking advantage of both singlets and triplet states [1], [16].

Non-radiative transitions: Non-radiative transitions essentially compete with fluorescence and phosphorescence. They correspond to vibrational relaxation and internal conversion which occur as result of nuclear interactions, in the range of 10^{-14} to 10^{-10} sec [1],[33].

Photo-induced Absorption: Refers to the absorption of a photon that brings state T_1 to higher triplet excited states (T_n). Photo-induced transient absorption experiments utilize this mechanism in order to track triplet excitons [1].

2.6.2 Intermolecular Energy Transfer

An exciton is possible to transfer its energy to another molecule through an energy transfer mechanism. There are three different energy transfer processes, namely radiative energy transfer or photon re-absorption, Förster energy transfer and Dexter energy transfer [1], [34].

Radiative Transfer: In radiative transfer, the photon emission takes place due to recombination of the exciton on the donor molecule, which is re-absorbed by the acceptor molecule. Typical distances, in which this process is possible to occur, correspond to a range of several 100 Å. A requirement for this to happen is existence of significant overlap in the emission spectrum of the donor molecule and the absorption spectrum of the acceptor molecule [1], [18], [33]–[35].

Förster Transfer: The Förster energy transfer process refers to an energy transfer from donor molecule to the acceptor and is based on a dipole–dipole electromagnetic interaction [1]. This mechanism takes place within an interval of 10^{-9} s and 10 nm distances [33]–[35]. Typically only singlet excitons can be transferred through this mechanism.

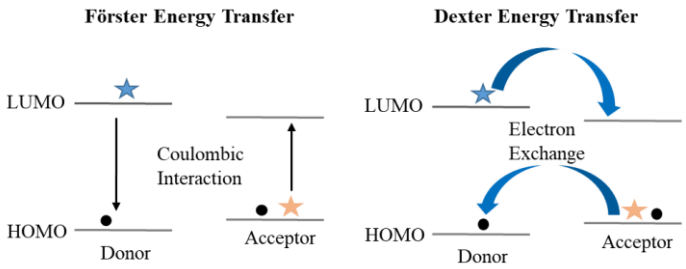

Figure 2.8: Illustration of energy transfer processes: Förster (left) resonance and Dexter (right) electron-exchange.

Dexter Transfer: The term Dexter Transfer refers to an energy transfer process that happens through an electron exchange interaction. This mechanism involves the exchange of an excited electron (via quantum mechanical tunneling) from the donor with one in the ground state from the acceptor. The contribution from a Dexter type energy transfer is only significant at very short distances, up to 1 nm. Both singlet and triplet excitons may be transferred through this mechanism [1], [39], [40].

2.7 Materials

Small Molecules

Small molecules (SMs) refer to materials with low molecular weight (molar mass approximately <1000 g/mol). One of the main advantages of SMs is the relatively simplistic control of charge transport by alteration of several molecular parameters. For instance and in comparison to polymer semiconductors , the capability of SMs to pack into high-ordered polycrystalline films gives rise to higher mobilities [3]. In addition, SMs offer several outstanding characteristics, such as exceptional EL and PL, high thermal stability, easy synthesis and purification. [41]. As a result, SMs are an attractive candidate for OLEDs. In Figure 2.9 is shown the structure of some of the most popular SMs that have been explored for applications in OLED devices.

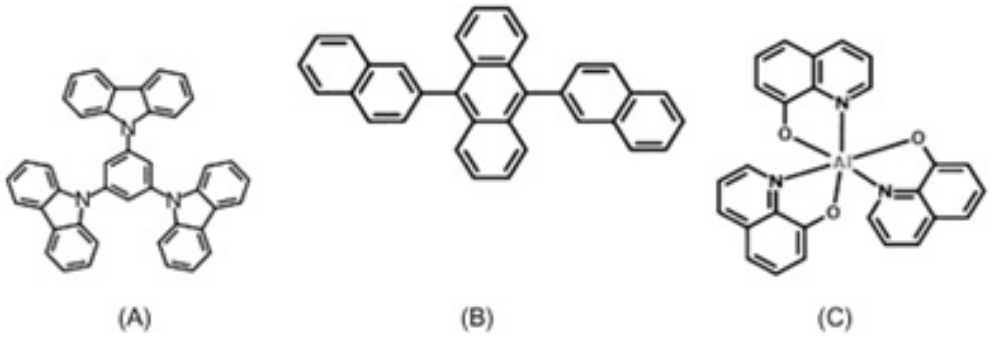

Figure 2.9: Structure of some popular small molecules. (A) 1,3,5-Tris(carbazol-9-yl)benzene; (B) 9,10-Bis(2-naphthyl)anthraces; (C) Alq3-Tris(8-hydroxyquinoline)aluminum [3].

However, many SMs are not always compatible with solution processing and often require more sophisticated techniques, such as vacuum thermal deposition [42]. Therefore, the development of SMs for solution processable OLEDs that are able to compete the evaporated analogue, it is very important. Especially, most of the studies regarding the blue emitters have explored molecules with excellent fluorescence characteristics, including anthracene and pyrene etc [42]–[44].

Polymers

Semiconducting polymers have been a very worthwhile material choice for the development of OLEDs [45]–[48]. Mainly due to possibility of simplified processes regarding the device production, using solution-based techniques (spin-coating etc.), leading to decrease in energy consumption [45].

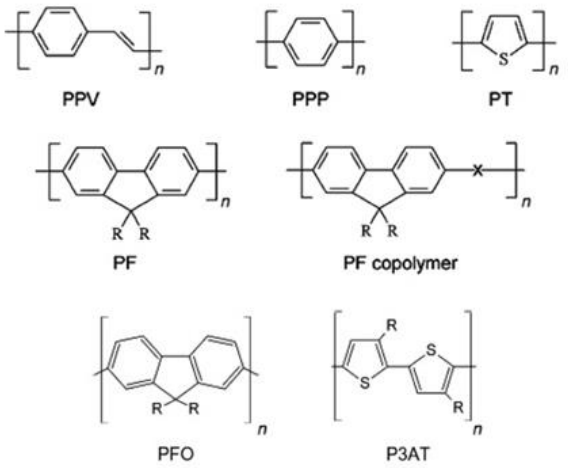

Figure 2.10: Chemical structures of some typical polymers for organic light emitting diodes: polyparaphenylenevinylene (PPV), polyparaphenylene (PPP), polythiophene (PT), polyfluorene (PF), and polyfluorene copolymers, polyfluorene (PFO); poly(3-alkylthiophene) (P3AT) [3].

Over the years, there has been an increasing interest and consequently more research activities have been developed in the field of Polymer Light Emitting Diodes (PLEDs) [45], [47], [48]. Studies were focusing on the design and synthesis of new polymeric materials, which would enable the improvement of luminous efficiency, color properties and device reliability. The chemical structures of some of the most-studied organic polymeric semiconductors are shown in Figure 2.10

Semiconducting, or “conjugated polymers”, are a suitable material choice because they combine superb charge transport properties and a high quantum efficiency for luminescence [49]–[51]. Conjugated polymers are distinguished as rigid rod-like polymers due to their π-conjugated backbone [52]. They exhibit complex morphology and phase behavior due to sensitivity in the presence of chemical defects, chain-chain interactions (π-stacking) and chain-solvent interactions [52]–[54]. The consequential structure and its

influence on π-stacking and other interactions, significantly affect the optical and electronic properties of the material [52].

Polyfluorene (PFO) is among the most well- known conjugated polymers in the field of PLEDs, especially for blue emitting device [48], [55]–[57]. PFO is a wide band-gap, highly fluorescent, bluish-green emitting polymer, having hole mobility ($\sim 10^{-5}$–10^{-4} cm^2 v^{-1} s^{-1}) [58]. In addition, it exhibits a high photoluminescence quantum efficiency (∼0.45–0.55), with good thermal and chemical stability [59].

2.8 Generations of OLEDs

In general, the three generations are divided into green, red, and blue emitters [4], [18]. The first generation of OLED utilized fluorescent materials as emitters. The second generation of OLEDs introduces the complexes which included heavy-metal dopants, such as iridium(III) and platinum(III). These complexes are able to harness both singlet and triplet excitons. Consequently, phosphorescent materials can achieve 100% internal quantum efficiency and as a result they are very attractive materials for OLEDs [36]. Literally, the exploration of phosphorescent revolutionized the field of displays and they are nowadays part of some of the most important media displays in use. Nonetheless, there are still several crucial drawbacks that need to be considered:

- The cost and limited resources of metals such as Ir etc.
- Highly-efficient and stable deep-blue phosphorescent emitters, remains a significant challenge. Regarding these devices, commercial applications still rely on phosphorescent emitters.

The third generation of OLEDs is based on thermally activated delayed fluorescence (TADF) mechanism. The TADF emitters utilized the reverse intersystem crossing (RISC) process, through which they are allowed to thermally reoccupy the singlet state from the triplet state. Similarly to phosphorescent emitters, TADFs can manifest both singlet and triplet excitons. However in the case of TADF, emission occurs from the singlet state and thus, triplet-triplet annihilation is significantly reduced. Hence, OLEDs based on TADF materials combine high efficiency and stability [36], [60].

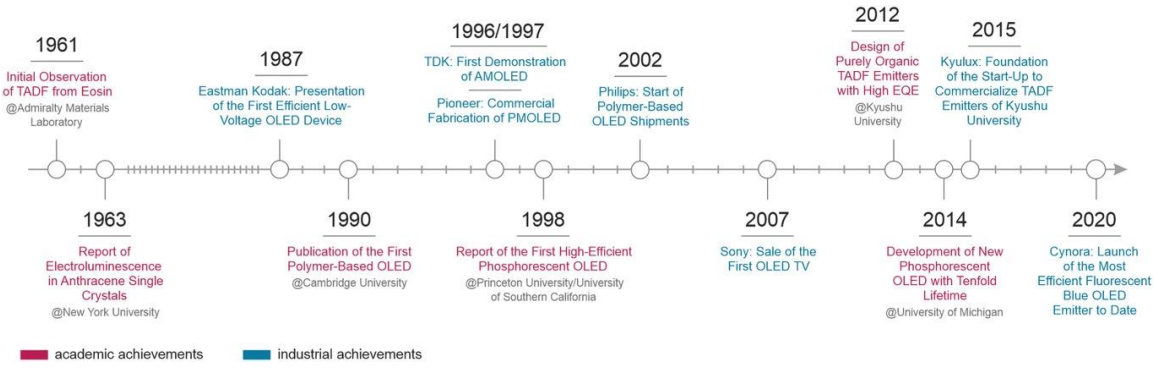

Figure 2.11: Overview of breakthrough discoveries in OLED technology [4].

Companies are steadily investigating new OLED materials, in order to improve the overall efficiency of existing OLEDs. Recently, CYNORA launched cyBlueBooster as a blue fluorescent emitter, which exhibits world record EQE compared to the customized blue emitter materials [61]. In spite the intrinsic limitation of fluorescent emitters which has already discussed, practical applications continue to depend on this class of materials. Consequently, it is vital to expand the scope of candidates for OLEDs and to explore new possibilities for next generation emitting materials [36].

Chapter 3: Experimental Methods

In this chapter, experimental processes are described in detail. Material selection, film and device fabrication as well as characterization, are all included.

3.1 Materials

Proper material selection is a crucial factor, which ensures balanced carrier injection and avoids exciton quenching. For this purpose, the most important criteria concerns the energy levels of organic or/and inorganic interfaces. HOMO and LUMO energy levels of respective materials should match, in order to achieve a high efficiency. Consequently, the choice of anode and cathode materials is also very important, as their work function values should match the HOMO and LUMO levels of the organic components. Taking all the above into consideration, we chose the following materials (see Figure 3.2) for the fabrication of OLED devices within this thesis:

Anode: Indium Tin Oxide (ITO) -coated glass substrates, purchased from XinYan Technology LtD, were used as anode material and substrate, respectively. ITO offers a plethora of attractive characteristics, such as suitable wok function, high transparency, appropriate conductivity, outstanding adhesion towards the substrates. As a result, ITO is the most widely used anode material [62], [63].

Hole transport layer: A transparent conductive polymer, P(3,4-ethylenedioxythiophene):poly(4 styrenesulfonate) (PEDOT:PSS) ,purchased from Heraeus Materials Technology, was used on top of the ITO. Essentially, it is a mixture of the ionomers poly(3,4-ethylenedioxythiophene) and polystyrene sulfonate. As a transport material it offers unique properties, such as transparency, conductivity, ductility and easy processing, simply via solution processing (spin-coating) [64].

Emissive layer: The conjugate polymer PFO (Sigma Aldrich) and the SMs TPAA and TPAP (synthesized by Dr. R.Hallani) constructed the emissive layer of the OLED devices which were fabricated in this thesis. Their molecular structures of these materials are shown in Figure 3.1. Usually, host-guest systems are introduece in order to enhance and control the intrinsic optical and thus, electronic properties of poly(fluorene). This can be achieved with various l strategies e.g. by using novel guests as small organic dyes. Following this approach, we introduce host:guest systems ,PFO:TPAA and PFO:TPAP, targeting to improve the properties of PLED devices and also to widen the spectral emission range.

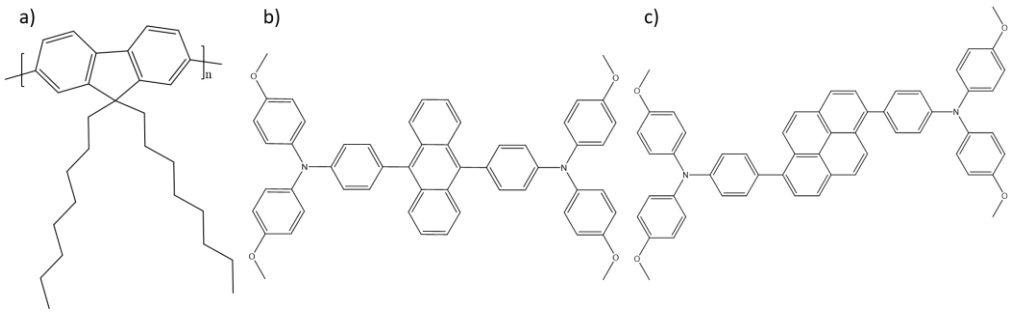

Figure 3.1: Chemical structures of a) conjugated polymer PFO- and small molecules b) TPAA and c) TPAP.

Electron Transport layer: Bathocuproine (BCP), purchased from Sigma Aldrich. BCP is a commonly used and in genersal suitable ETL material. As can be seen in Figure 3.2, it is a wide bang gap (Eg) materials. In addition to the shallow LUMO level of -2.9 eV it also has a deep HOMO level, which is good for hole blocking properties.

Cathode: Metallic silver (Ag**)** was utilized as cathode material.

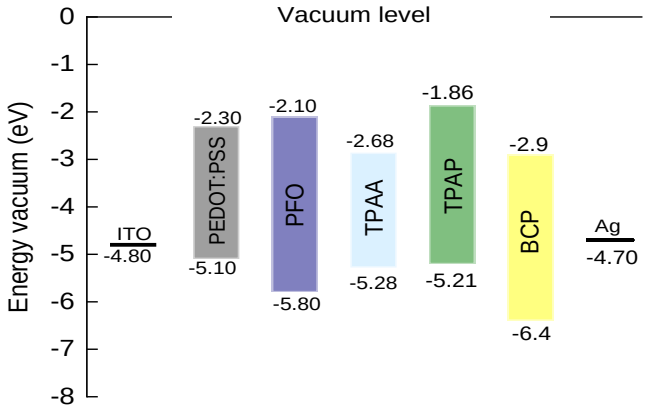

Figure 3.2: Schematic HOMO-LUMO energy level diagram of OLED materials used in the current study. HOMO and LUMO levels as measured from PESA/UV-Vis absorption (for PFO, TPAA, TPAP) and as mentioned in the literature (ITO, PEDOT:PSS, BCP, Ag) [5], [6].

3.2 Substrates Preparation

In advance of the device fabrication, ITO-coated glass substrates of 10 Ohm/sq were thoroughly cleaned. The cleaning sequence included consecutive ultrasonic baths in detergent, de-ionized water (DI), acetone and isopropanol, each for 15 minutes, followed by a dry blowing step using a nitrogen (N_2) gun. The final performance of the OLED devices, strongly depend on the surface properties of ITO. For this reason,

a UV-ozone treatment was used for 20 minutes, in order to increase the work function and hole-injection capability of ITO [63].

3.3 Solutions Preparation

Host:guest mixtures of PFO:TPAA, with a total concentration of 10 mg mL-1 were dissolved in o-xylene. Blends of PFO:TPAP with a total concentration 10 mg mL-1 were also dissolved in o-xylene. Additionally, PFO was dissolved in o-xylene in a total concentration of 10 mg mL-1. All solutions where stirred and heated overnight at 60 °C.

3.4 Device Fabrication

Onto the clean ITO substrates, the PEDOT:PSS HTL was deposited by spin-coating the solution in the air at a speed of 4000 rpm for 30 seconds. This, resulted in an approximately 30 nm thick layers. This layer was subsequently thermally annealed at 150℃ for 15 minutes in air. The EML solutions were spin-coated atop the PEDOT:PSS layer at 2000 rpm, inside a nitrogen filled glove box, then baked at 80℃ for 10 minutes. Thereafter, the samples were transferred into a thermal evaporation system where BCP (10 nm) and Ag (100nm) were deposited through a shadow mask with an active device area of 10 mm^2. All depositions were carried out by vacuum thermal evaporation in a system made by Angstrom Engineering, at pressure below 2×10^{-6} Torr. The final device structure consisted of ITO/PEDOT:PSS (30 nm)/EML (60nm)/BCP (10 nm)/Ag (100) nm. Based on the

different EMLs and for different PFO:SMs ratios, the obtained devices are shown in Table 3.1 below.

Table 3.1: Composition of the emissive layer of the various fabricated OLED devices.

Device	Emissive layer	ratio wt%
A	PFO:TPAA	50:50
B	PFO:TPAP	50:50
C	PFO:TPAA	95:5
D	PFO:TPAA	80:20
E	PFO	-

3.6 Device characterization measurements

3.6.1 Current Density-Voltage-Luminescence Characterization

Fabricated devices were characterized by current–voltage–luminescence using a Keysight B2912A source meter and Konica Minolta LS-150 Luminance meter, controlled with a custom-made software build in MATLAB. A spectrometer (Ocean Optics, QE65000) and a 2'' integrating sphere (Thorlabs, IS236A) were used in order to obtain the EL spectra of the OLEDs. All the measurements were performed under N_2 atmosphere inside a glovebox.

The current density (**J**) was calculated from the recorded current (I), divided by the active area of the device (10 mm^2) via:

$$J = \frac{I[A]}{10 \cdot 10^{-6}} = I[mA] \cdot 10^2 \frac{A}{m^2} \quad (3.1)$$

3.6.2 Chromaticity Measurements

Chromaticity of a lighting source is most commonly described using the 1931 Commission Internationale de l'Eclairage (CIE) system. As it is shown in Figure 3.3, this system consists of a horseshoe-shaped diagram that contains all the colors that the human eye can detect.

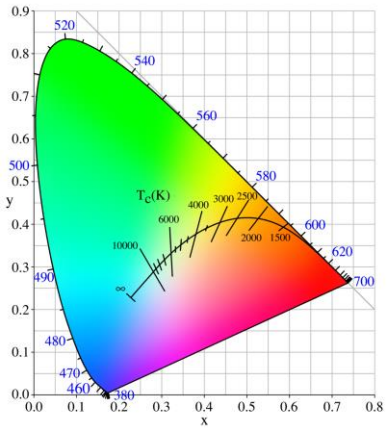

Figure 3.3: Typical CIE 1931 chromaticity diagram [7].

The outer border contains all monochromatic colors. The curved line in the interior of the CIE diagram is the Planckian locus, which denotes the observed color of a blackbody radiator at the indicated temperature. Any color within the CIE diagram can be reproduced using an appropriate combination of the CIE primary colors red, green and blue (RGB) [7]. In the perimeter of the chromaticity diagram, monochromatic emissions can be detected. Regardless, as the width of the source becomes broader, the x and y values fall towards the center. From such coordinates we can extract and compare the color purity of our OLEDs as follow:

$$\text{Color purity} = \frac{\Phi}{\Phi+\delta} = \frac{\sqrt{(x-x_{ee})^2+(y-y_{ee})^2}}{\sqrt{(x_d-x_{ee})^2+(y_d-y_{ee})^2}} \quad (3.2)$$

where δ and Φ are the distances from the dominant wavelength (the wavelength located at the perimeter of the chromaticity diagram) to the source and to the equal energy point, respectively. (x, y), (x_{ee}, y_{ee}), (x_d, y_d) are the source, equal point and dominant wavelength coordinates. It is noted that, usually, a 100 % color purity is obtained for monochromatic sources and near 0% for a white source [65].

Chromaticity measurements were performed together with all the current–voltage–luminescence measurements that were mentioned before and the values were obtain using a custom-made code build in MATLAB.

3.6.3 Impedance Spectroscopy measurements

A practical and non-destructive method which can be used for the characterization of the electric properties of the materials and their interfaces, is known as Impedance Spectroscopy (IS). In the case of OLEDs, which are double carrier devices, IS can be employed in order to study the charge transport kinetics, as well as the relaxation processes [66].

In a typical OLED IS experiment, the device is modelled in terms of equivalent circuits, with resistance (R) and capacitance (C) referred to as RC circuits. Multi-layered OLEDs, such as the devices fabricated in the current work, can be represented by the parallel connection of the resistance (R_p) and capacitance (C_p) of the organic layers and by the contact resistance (R_c) in series. The impedance (Z) is expressed as a function of angular frequency (w):

$$Z = R_c + \frac{R_p - jwR_p^2C_p}{1+w^2R_p^2C_p^2} = Re(z) - jIm(z) \quad (3.3)$$

$$\text{Where } Re(z) = R_c + \frac{R_p}{1+w^2R_p^2C_p^2} \quad (3.4)$$

$$Im(z) = \frac{wR_p^2C_p}{1+w^2R_p^2C_p^2} \quad (3.5)$$

The frequency of the applied voltage greatly affects the impedance of the device. In high frequencies, only the real part is considered, since the imaginary part becomes almost negligible. As a result, low frequency regions can successfully implemented in order to study the capacitance and resistance of the organic layers [28].

One common representation of an IS experiment results is the Cole-Cole plot of the modulus. In such a plot the conductive characteristics of OLEDs can be revealed, showing the capacitance as a function of the frequency in polar coordinates.

IS measurements were conducted using a frequency response analyser (Solartron 1260A). During the measurements, a 10 mV AC signal is applied without DC bias in the frequency range of 1 MHz to 1 Hz, under N_2 atmosphere inside a glovebox.

3.7 Film characterization measurements:

For all the EML film characterization measurements, solutions (see Table 3.1) were spin-coated at 2000 rpm on top of plain glass substrates.

3.7.1 Absorption Measurements

In a first approximation the attenuation of a light beam that passes through matter can be described by the Beer-Lambert law:

$$I=I_o \cdot e^{-\alpha \cdot d} \quad (3.5)$$

Where I_0 is the intensity of the light beam before travelling through matter, I is the intensity after the passing, α is the absorption coefficient of the sample and d the length of the optical path in the material.

Absorption spectra of thin films were measured by UV-VIS spectrophotometer (Cary 5000).

3.7.2 Steady State Photoluminescence

Photoluminescence spectra were acquired by a HORIBA Fluroromax-4 Horiba spectrofluorophotometer, using a custom made sample holder, designed for thin films.

3.7.3 Time-Resolved Photoluminescence

For Time-Resolved Photoluminescence (TR-PL) experiments, the samples were excited with the Chameleon Ultra laser (Coherent) at 410 nm with a pulse width of 140 femto-seconds (fs) and a repetition rate of 80 MHz. Typical pulse energies were in the range of 100 μJ. The PL of the samples were collected by an optical telescope (consisting of two plano-convex lenses), and it was further focused on the slit of a spectrograph (PI Spectra Pro SP2300), and eventually detected with a Streak Camera (Hamamatsu C10910) system with a temporal resolution of 140 fs. The

data was acquired in photon counting mode using the Streak Camera software (HPD-TA), and was exported to Origin Pro 2019 for further analysis.

3.7.4 Photoelectron Spectroscopy in Air

In an organic material, the energy of the HOMO and LUMO are essentially equivalent to the ionization potential (IP) and electron affinity (EA) respectively. The IP corresponds to the energy which is necessary in order to promote an electron from the HOMO to the vacuum level. The EA is described as the least energy required for an electron so as to occupy the LUMO of a molecule, through vertical transition from the vacuum level. The HOMO and LUMO are often estimated from UV/Vis absorption/photoluminescence spectroscopy for the optical gap if required [67], [68].

The IP of the thin films was measured by photoelectron spectroscopy in air (PESA). The optical gap was measured using UV/Vis absorption, from which finally the electron affinity was estimated.

3.7.5 Atomic Force Microscopy

Atomic force microscopy (AFM) is a very powerful tool that can be used in order to investigate the three dimensional surface morphology, with the resolutions up to nanometer(s). A sharp force probe (cantilever) is used facilitates the measurement of surface height at each point (2D) of the sample [69]. During the measurement it is possible that the cantilever moves over a stationary sample or it may remain static and the sample moves under the probe. One approach to ensure a non-destructive study of the sample, is the implementation of intermittent contact. Most commonly, the so called “tapping

mode" is used. In tapping mode, the cantilever oscillates approximately at its lowest resonant frequency. The tracking of surface topography is acquired through control of the cantilever's amplitude of oscillation. The term tracking refers to Z scanner that reactively adjusts the distance between oscillating tip and sample as the tip amplitude is kept constant.

In this work, surface roughness and topography of thin films based on different blends (see Table 3.1) were examined using Bruker Dimension Icon with ScanAsyst. AFM images were obtained using tapping mode at scan size of 1 μm, drive frequency of 133.9 kHz and drive amplitude of 306.1 mV.

3.7.6 Transmission Electron Microscopy

Transmission electron microscopy (TEM) is one of the most versatile techniques can study and visualize the local microstructure of the material. During a TEM experiment, an electron beam is transmitted through the thin samples. The resulting interactions between the electron beam and sample, generate images that are in general characterized by high resolutions [70].

To acquire the top-view transmission electron micrographs (TEM) the studied films were spin-coated on glass substrates, on which also PEDOT:PSS was spin-coated. Following the spin-coating processes, the samples were placed in DI water and the films were floated off and finally collected on lacey carbon coated TEM grids (Electron Microscopy Sciences), using the so called "fishing" method. TEM images were obtained with a FEI Titan 80-300 microscope operating at 300 keV, using a 4k x 4k eagle CCD camera (FEI).

3.7.7 Hyperspectral Luminescence Imaging Microscopy

Hyperspectral Microscopy is a cutting-edge technique which essentially integrates hyperspectral imaging with advanced optics and computer software. Consequently, it enables the fast analysis of materials at the micro or even nanoscale [71]. The term Hyperspectral is preferred instead of spectral, due to the range of the wavelengths that is possible to be used, which typically includes near-infrared, visible and often even ultra-violet spectra. Each 2D surface image is acquired at a limited range of the spectrum. The monochromatic images obtained, result in the so called data cube, which accommodates the spatial and spectral details of the studied specimen. The x and y dimensions of the data cube correspond to the spatial information and the z axis is linked to the wavelength. For each point of this data cube, the light intensity is registered. It is possible to present the data in two ways: a) 2D monochromatic images for respective wavelengths and b) PL spectrum for a chosen spatial position.

In the current work, the data were acquired by Hyperspectral Microscope, IMA Fluorescence (Photon etc.), where a laser of 532 nm was used as excitation light source.

3.8 Theoretical Calculations: Density Functional Theory

One of the most well-known simulation methods in the field of materials science, is the Density functional theory (DFT). This method is a quantum mechanical modelling which enables the investigation of the electronic structure of many-body systems, in particular atoms or molecules and the condensed matter. The basis of DFT introduces the idea of

using only the density, in terms of functionals, as the basic variable in order to determine the properties of a many-electron system [72], [73].

DFT calculations were carried out in order to obtain the HOMO and LUMO energies and plots. Specifically, the NWChem code [74], the hybrid B3LYP exchange-correlation (xc) functional [75], [76] and the DZVP orbital basis were used [77]. To include the effect of the solvent (o-xylene) on the HOMO and LUMO energies the COSMO model was utilized [78]. The reported HOMO energies are the results of the DFT calculations. The reported LUMO energies, on the other hand, were obtained by adding to the HOMO energies the corresponding energy differences between the ground state and the first excited singlet state, which were calculated within the Tamm-Danncoff Time Dependent DFT approach [79]. Structures and HOMO/LUMO plots were rendered with VESTA [80]. To model PFO a tetramer segment was used.

Chapter 4: Results and Discussion

4.1 Device Performance

Organic light emitting diodes utilizing an EML consisted of PFO as a host and SMs TPAA and TPAP as guests, were fabricated and tested. Optimized devices followed the structure, ITO/PEDOT:PSS/EML/BCP/Ag (see Figure 4.1-a). Turn on voltages for each device were acquired from Current density- Luminance- Voltage data (see Figure 4.1-b). The maximum luminance of 13600 at 7.5 volts is obtained for the PFO:TPAA device, which corresponds to our best device. For the PFO: TPAP based device, maximum luminance 7000 cd/m^2 is obtained at 7.5 volts. Both blends show luminance enhancement, since the device based on PFO only EML was found to have maximum luminance of 4700 cd/m^2 at 7 volts. Moreover, the introduction of SMs guests TPAA and TPAP, leads to turn- on voltage reduction, from 4.25 volts to 3.39 volts and 3.90 volts respectively. The lower threshold voltage is likely attributed to smaller injection barrier. Also current density values of the blend systems is higher than the pure PFO device, for which we obtained maximum of 200 mA/cm^2 at 7 volts. The system of PFO:TPAA exhibited maximum of 690 mA/cm^2at 7.5 and the PFO:TPAP showed maximum of 333 mA/cm^2 at 7.5 volts. Similar behavior is observed in the EQE and current efficiency. Remarkably, the maximum EQE of both blend systems is significantly higher compared to the reference device, with the PFO:TPAA system exhibiting maximum EQE of 2.58 %, which is approximately 6.5 times the maximum EQE of PFO (0.4 %) based device. Also the maximum EQE 1.38% of the PFO:TPAP based OLED, is higher compared to the pure PFO device. Additionally,

compared to previous studies of OLEDs based on polymers and SMs, herein fabricated devices showed increased performance (Appendix A).

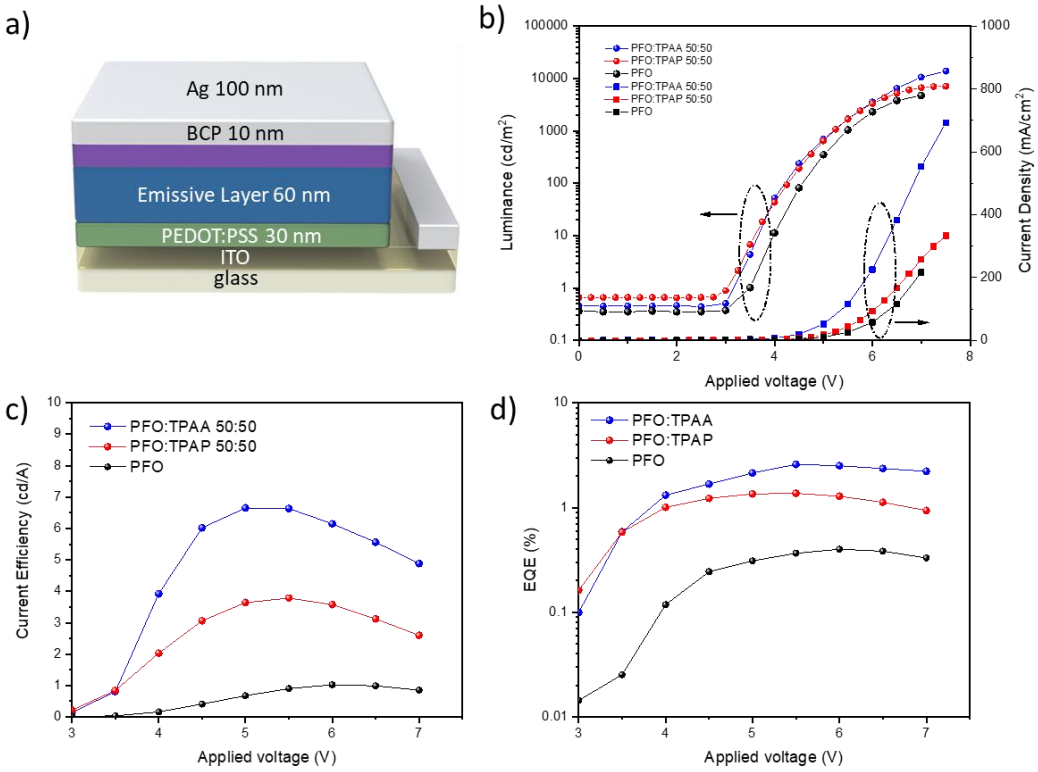

Figure 4.1: a) Final device structure of fabricated OLED devices. Emissive layer refers to different blends based on PFO and small molecules TPAA and TPAP as well as reference PFO only device – b) Current density- Luminance- Voltage characteristics of optimized devices based on systems of PFO:TPAA, PFO:TPAP ,PFO for which we obtained maximum luminance of 13600 cd/m^2 ,7000 cd/m^2 and respectively cd/m^2- c) Current efficiency results of the same devices correspond to 6.65 cd/A (PFO:TPAA), 3.78 cd/A (PFO:TPAP) and 1.02 cd/A (PFO).

For comparison, the device characteristics of all fabricated devices are summarized and presented in Table 4.1. The higher performance of the blends in comparison with pure PFO OLED devices, it is assigned to the better balance between electrons and holes along with charge confinement [81].

Table 4.1: Device performance results of optimized OLEDs devices.

Emissive layer	max Luminance (cd/m^2)	max Current density (mA/cm^2)	max Current efficiency (cd/A)	max EQE %
PFO	2600	216	1.02	0.40
PFO:TPAA	13600	691	6.65	2.58
PFO:TPAP	7000	333	3.78	1.36

4.2 Impedance Analysis

Similar behavior was observed in the impedance measurements in which single RC network is found to be adequate to simulate the Cole-Cole plots of the devices, indicating that bulk region is dominant on the device performance [82]. The acquired impedance data are presented in Figure 4.2, from which the parallel capacitance and parallel resistance data were obtained. We found C_p=4.51E-9 for PFO:TPAA based system and C_p=4.6E-9 for PFO:TPAP. For the parallel resistance, we found R_p=4.66E5 for PFO:TPAA based device, over the parallel resistance of the PFO:TPAP based system which showed R_p=5.31E5.

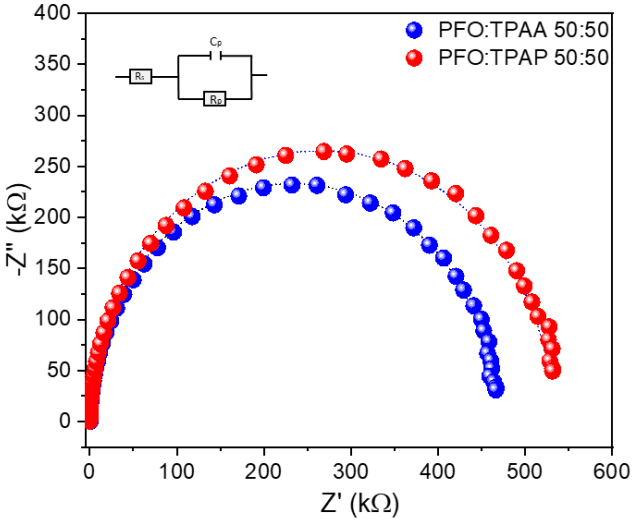

Figure 4.2: Measured (dots) and simulated (dashed line) Cole-Cole plot of the OLED devices based on PFO:TPAA (blue) and PFO:TPAP (red) active layers. Single RC network was used for simulated the device. Equivalent electrical circuit of the OLED device is illustrated (inert graph), where Rs refers to the series resistance due to the contacts, Rp and Cp correspond to the resistance and geometric capacitance of the intrinsic layer.

Capacitance measurements can implemented in order to examine the occupation of trap sites due to space charge effects [83], [84]. There are various factors that can affect the value of capacitance. Numerical simulations have shown that slow traps can increase the capacitance at low frequencies [85], [86]. In addition, the presence of slow ionic charges result in increased capacitance at low frequency regime. Recombination of charge carriers leads decreased capacitance, in which case it is possible to even obtain negative values [83], [87]. In our study we observed that PFO:TPAP system shows higher capacitance than the PFO:TPAA. Based on the above, we conclude that the increased capacitance in the case of PFO:TPAP system is due to existence of trap states. While the lower capacitance

value of the PFO:TPAA is due to effective charge carrier recombination, which results in enhanced device performance.

4.3 Electroluminescence characteristics

Interestingly, the examined EL spectra of OLED devices based on the two different types of EMLs showed no significant difference. PFO:TPAA (50:50) and PFO:TPAP (50:50) systems, exhibited EL spectrum peaks at 492nm and 497nm respectively (Figure 4.3). Comparison between the neat PFO EL emission and the blends explains this observation. When PFO is mixed with the SMs, the contributions of the main peak of pure PFO (444 nm), is reduced significantly, resulting in a small shoulder in both blends. Moreover, the two smaller peaks of neat PFO EL emission (477 nm and 518 nm), in the case of PFO:TPAA and PFO:TPAP blends appear as a main peak. All these provide speculations, as it will be discussed in detail in a following section, for energy transfer from PFO to TPAA and TPAP.

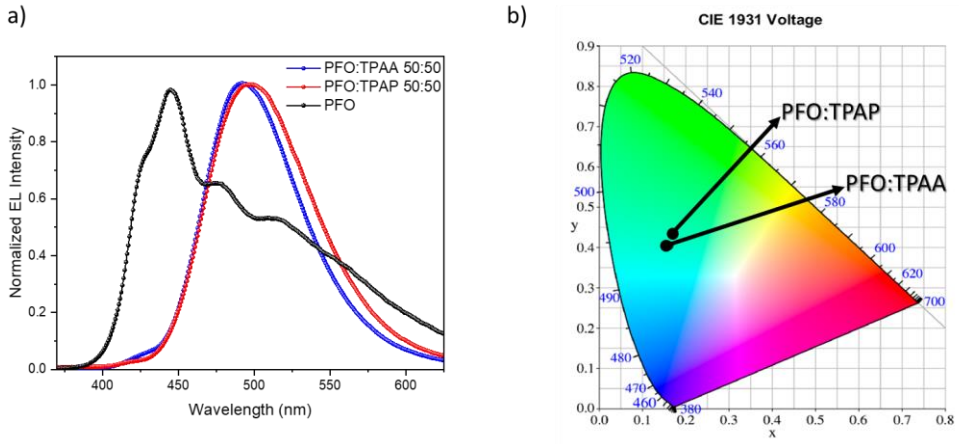

Figure 4.3: a) Electroluminescence spectra of fabricated OLEDs, as obtained at 7.5 applied voltage: PFO exhibits main emission at 444 nm with two smaller peaks at 477 nm and 518 nm, PFO:TPAA blend shows an emission peak at 492 nm and PFO: TPAP demonstrates emission at 497 nm – b) Chromaticity diagram of OLEDs based on the PFO:TPAA and PFO:TPAP EMLs. Chromaticity

coordinates for PFO:TPAA and PFO:TPAA systems correspond to (x=0.168, y=0.405) and (x=0.172, y=0.435) respectively.

The spectrum of the PFO: TPAA device results in CIE coordinates of (x=0.168, y=0.405). CIE coordinates of (x=0.172, y=0.435) obtained for the PFO: TPAP device (see Figure 4.4). Through equation 3.2, we obtained a color purity of 0.27 for the PFO:TPAA device and 0.22 for the PFO:TPAP system.

As mentioned above, PFO:TPAA and PFO:TPAP systems exhibit nearly identical EL behavior. However, the intensities of EL are the highest in the case of PFO:TPAA system (Figure 4.5). The spectrum of the PFO:TPAA device results in CIE coordinates of (x=0.168, y=0.405) in comparison with CIE coordinates of (x=0.172, y=0.435) for the PFO:TPAP device where both corresponds to the sky blue zone of the CIE 1931 color space. We observed no variation of the EL spectra as a function of the applied external voltage (Figure 4.4), which provides evidence for the stability of the electronic properties of our PFO:TPAA and PFO:TPAP emissive systems.

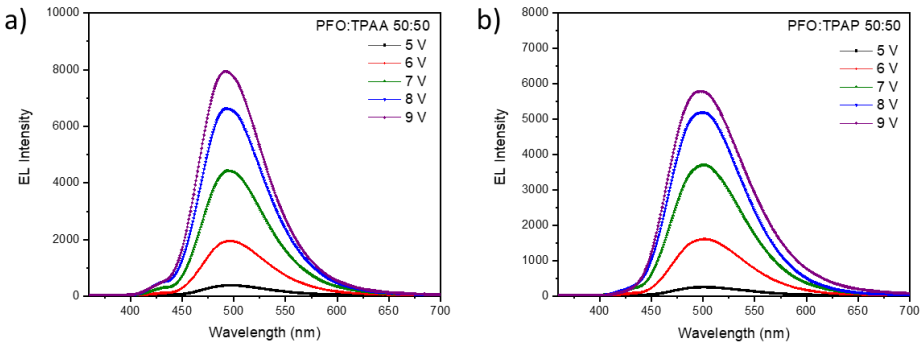

Figure 4.4: EL spectra as a function of the applied external voltage for a) PFO:TPAA - and b) PFO:TPAP systems. No variation was observed, indicating the operating stability of the fabricated organic light emitting diodes.

Investigations of EL emission for various doping conditions, regarding the PFO:TPAA EML based OLED, are presented in Figure 4.5. For doping concentration of 90:10 we observed a main peak at 476 nm with a shoulder at 456 nm and a smaller shoulder at 426 nm. Higher doping concentration of 80:20, showed a peak at 486 nm, with a shoulder at 426 nm.

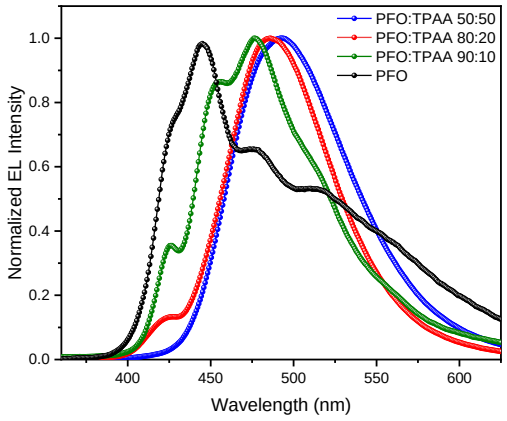

Figure 4.5: EL emission spectra of OLED devices based on PFO: TPAA EML, for different doping conditions. Increasing TPAA concentration results in red-shift.

The observed red-shift with increasing doping concentration can be attributed to energy transfer from the host to the dopant.

4.4 Absorption and Photoluminescence

The results of the examined UV-Vis absorption spectra of thin films based on the pristine PFO, TPAA and TPAP films as well as their blends for 50:50 concentration, are displayed in Figure 4.6-a below. PFO film spectrum exhibited a band at 385 nm. Pure TPAA film exhibited two bands located at 306 nm and 408 nm and two small shoulders at 360 nm and 382 nm. TPAP film showed two peaks, located at 303 nm and 413, as well as three shoulders. One shoulder at 369 nm and two smaller shoulders located at 348 nm and 388 nm respectively. PFO:TPAA blend showed two bands, the main one located at 394 nm and one at 310 nm. For the case of PFO:TPAP, two bands exhibited at 393 nm and at 306 nm.

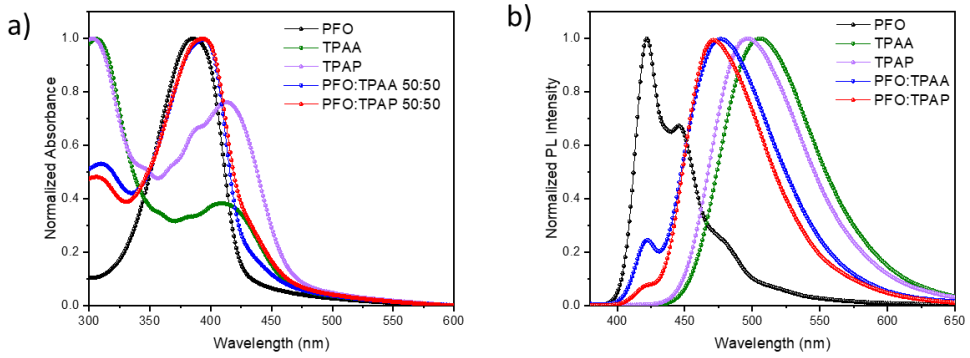

Figure 4.6: a) Absorption spectra – and b) Steady State Photoluminescence (PL) spectrum of thin films based on PFO, TPAA and TPAP- and PFO:TPAA (50:50) and PFO:TPAP (50:50) blends.

The main band of pure PFO film at around 385 nm, originates from the inhomogeneous broadened transition from So to S1, related to PFO α phase [88]. The same band is red-shifted in the case of PFO:TPAA and PFO:TPAP blends, since they appear at 394 nm and 393 nm respectively. This red-shift is attributed to the formation of aggregations, which has been confirmed by previous works [89]. We suspect that these aggregates are attributed to the existence of β phase of PFO.

Steady state PL results, for the thin films mentioned above, are shown in Figure 4.6-b. The pristine PFO film shows two emission peaks at 420 nm and 446 nm and a small shoulder at 470 nm. Pristine TPAA and TPAP films, exhibited peaks at 506 nm and 497 nm respectively. For the PFO:TPAA blend, we observe one peak at 476 nm, whilst the PL spectrum for the PFO:TPAP blend shows a peak at 471 nm. PFO:TPAA film showed two peaks, one at 477 nm and one at 422 nm. The PFO:TPAP film showed one main peak at 471 nm and a small one at 421 nm. The main band at 420 nm of PFO film, corresponds to 0-0 vibronic progression. The two bands appearing at 446 nm and 470 nm are associated to 0-1 and 0-2 vibronic transitions respectively [48], [90]. When PFO is doped with either TPAA or TPAP, the contribution of PFO in the emission of PL spectra decreases significantly. The main band of PFO, in the case of PFO:TPAA and PFO:TPAP blends appears as a shoulder at approximately 424 nm. At the same time, the contribution of the TPAA and TPAP resulting at 476 nm and 471 nm respectively, is dominant. During doping, some dopant states remain optically un-excited. Hence, energy can be transferred through Förster mechanism to the SMs TPAP and TPAP, from the singlet states of PFO.

As a result, the contribution of PFO emission is significantly decreased [91]. This statement is also confirmed by the sufficient overlap between the PL spectrum of the host PFO and the absorption of the dopants TPAA and TPAP (see Appendix C).

4.5 Investigations of Structure-Properties Relationship

The performance of the pyrene based system (device B), is relatively lower compared to the anthracene one (device A). Enhanced device performance can be assigned to the different morphological characteristics of the films, which are of course affected by the film forming processes (solvent, annealing temperature etc). AFM and TEM studies, combined with HLM analysis, gave insights to the structure-properties relationship.

AFM analysis (Figure 4.7) gave insights regarding the morphology of the thin films based on the two different blends, under 50:50 doping condition. For PFO:TPAA based films we obtained Root-mean-square (RMS) roughness with an average R_{RMS}= 1.01 nm and for the PFO:TPAP based thin films, R_{RMS}= 1.90 nm was acquired .

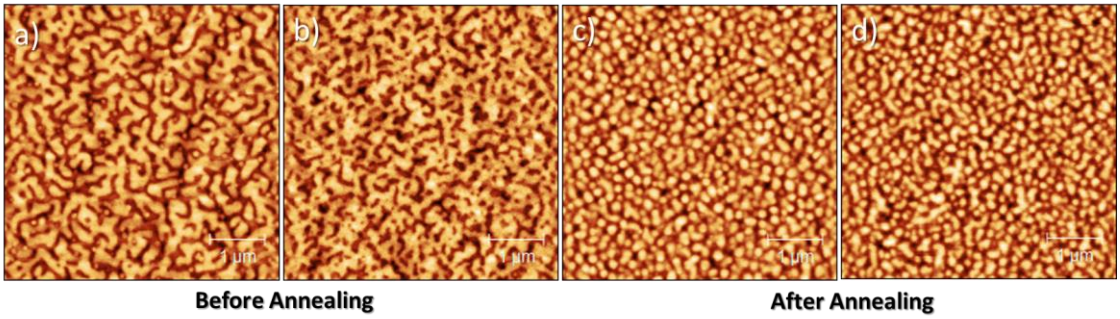

Figure 4.7: AFM images of as cast films of (a) PFO: TPAA – (b) PFO: TPAP and annealed thin films of (c) PFO: TPAA – (d) PFO: TPAP.

For as cast films, we observed in both cases, the existence of phase separation. However, PFO:TPAA system appears to have higher degree of conjugation and more well-formed rod-like conformations. Whilst, in the case of PFO:TPAP system, the rod-like domains form island-like structures, separated by longer distances. After annealing at 80 ℃ for 10 minutes, in both systems we observed a very different morphology. It seems that annealing promotes the blending and both systems are more well-blended compared to the as cast systems. Although, PFO:TPAA blend is more aggregated while in the PFO:TPAP the domains yet seem to be separated by longer distances again. This is also linked to

Impedance results (see Figure 4.2) which revealed that PFO:TPAP device is more trapping compared to PFO:TPAA device. In Figure 4.8 we present a schematic illustration of the annealing effect on the aggregations of PFO:SM system, supported also by previous studies [92]. Overall, the aggregation observed in the films, provides an efficient charge-transport channel, which results in an increased current efficacy.

Conjugated polymer PFO appears in five different phases, depending on the side-chain structure and annealing temperature: α phase (disordered glassy phase), β phase (crystalline), γ phase, amorphous and nematic [52]. In general, β phase (its existence is suspected by the presence of an additional absorption peak at 437 nm), is a highly ordered conformation, with a higher conjugation length compared to phase α, which favors charge carrier transport [88].

PFO molecules consist of interdigitated side chains. Thermal annealing enhances the interaction of intra-chain and inter-chain of PFO, which exhibits the evolution of PFO main

chain with planar conformation [88]. This gives adequate time to PFO chains to bind to the crystallization front. Concurrently, the crystal growth and π-π stacking time interval elevate. In this way, PFO molecules acquire a disorder-order transition. Moreover, the formation of ordered aggregation is promoted. Also previous studies [88], [93] showed that exposure to poor solvent or annealing treatment might lead to *β* phase formation

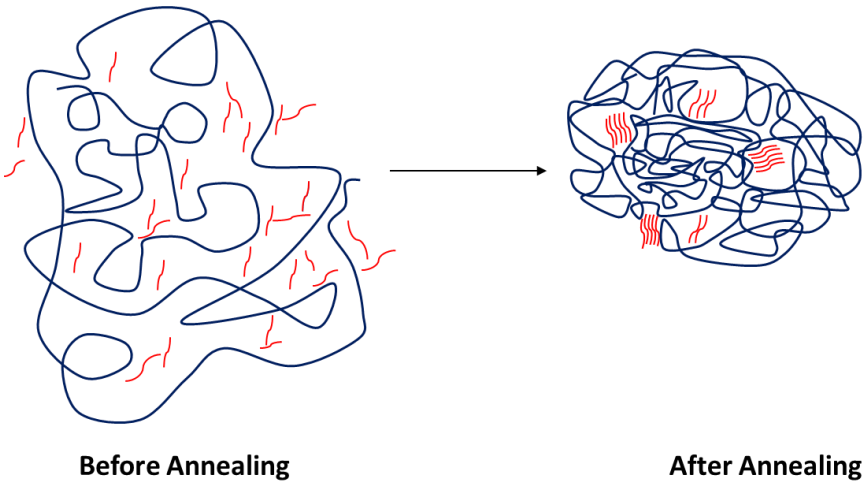

Figure 4.8: Schematic illustration of the chain configuration and microstructure annealing effect upon blending the conjugating polymer PFO (shown as dark blue elongated lines) with a small molecule, either TPAA or TPAP (represented by short red line segments). Before annealing PFO chain exhibits its glassy (disorder) state. After annealing, PFO chain entangles and phase transformation (β phase) occurs. Small molecules obtain higher packing arrangement.

However SMs behave differently than polymers. They are more rigid and with annealing, they do not entangle as the polymers do [43]. As illustrated in the Figure 4.1 above, SMs alter their packing density. Looking now into the chemical structures of our SMs TPAA and TPAP (see Figure 3.1), we observe that they are almost alike, except the anthracene and pyrene unit respectively. In general, anthracene is known to be more soluble than pyrene [94] and this explains why TPAA forms better blends with PFO, compared to TPAP.

TEM analysis revealed similar trend (Figure 4.9). As cast films based on PFO:TPAA exhibits well-formed and oriented domains compared to the PFO:TPAP blend. After annealing, thin films of PFO:TPAA seem to form larger and more aggregated domains compared to the PFO:TPAP system. Moreover, PFO:TPAA blend forms not only larger but also darker (denser) aggregations, compared to the PFO:TPAP system. The ordered domains of PFO:TPAA system occupy less volume, resulting in a planar and highly packed compared to PFO:TPAP.

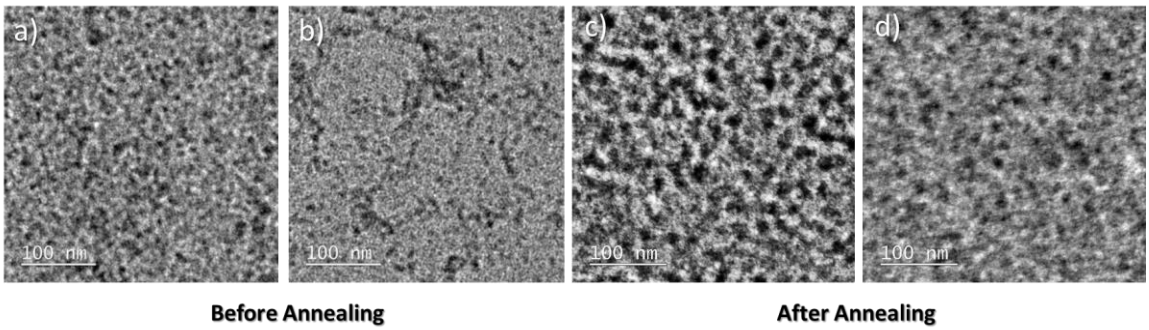

Figure 4.9: TEM images of as cast films of (a) PFO: TPAA – (b) PFO: TPAP and annealed thin films of (c) PFO: TPAA – (d) PFO: TPAP.

In addition to above studies, HLM measurements were carried out in order to determine if this aggregations are beneficial or detrimental for this device (Figure 4.10). HLM analysis clearly showed that strong emission arises from the large domains of the PFO:TPAA systems which results in homogenous and smoother films. In contrast, in the case of

PFO:TPAP blend only the small domains contribute in the emission.

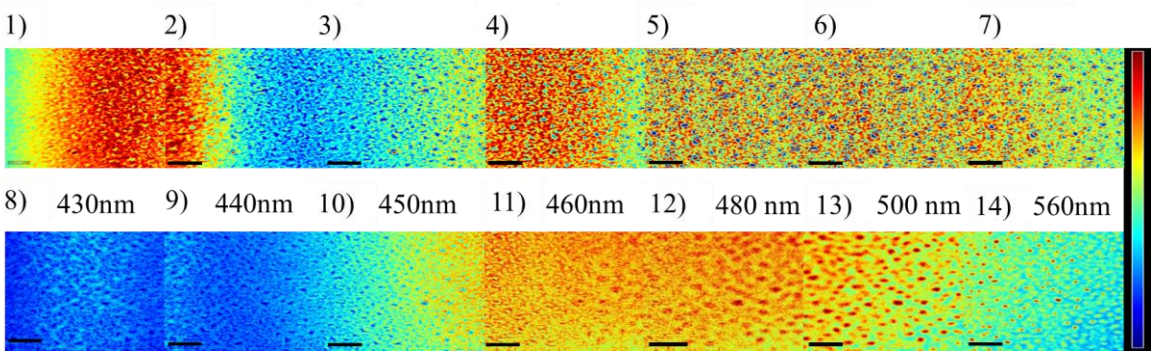

Figure 4.10: Hyperspectral Luminescence Microscopy Images of PFO:TPAA (a-g)- and PFO:TPAP (h-n) films extracted at the defined wavelength (nm). Scale bar indicates photoluminescence (PL) emission intensity.

Based on the increased level of aggregates as well as on previous studies [54], [95]–[97], we suspect that annealing treatment results in polymer chain β phase transformation of the polymer PFO. Especially in the case of annealed PFO:TPAA the level of aggregation is significantly increased. These aggregates act as nucleation centers and promote β phase. Moreover, previous works claim that the fraction of β phase affects the production of polarons and triplet excitons as well as the photoluminescence quantum efficiency [52], [54], [88]. Overall, annealed PFO:TPAA system is more well-blended than PFO:TPAP and, this explains the significantly higher performance of this system. This is also supported by the obtained root-mean-square (RMS) roughness values of films, which show that TPAA based films are smoother (average R_{RMS}= 1.01 nm), compared to TPAP based film which showed almost doubled value (R_{RMS}= 1.9 nm).

4.6 Theoretical Studies

To obtain a better understanding of the properties of SMs TPAA and TPAP and PFO, their HOMO and LUMO energy levels were estimated using DFT calculations (Figure 4.11) and experimental techniques. In general, DFT and experimental are found to be in a satisfactory agreement (see Table 4.1).

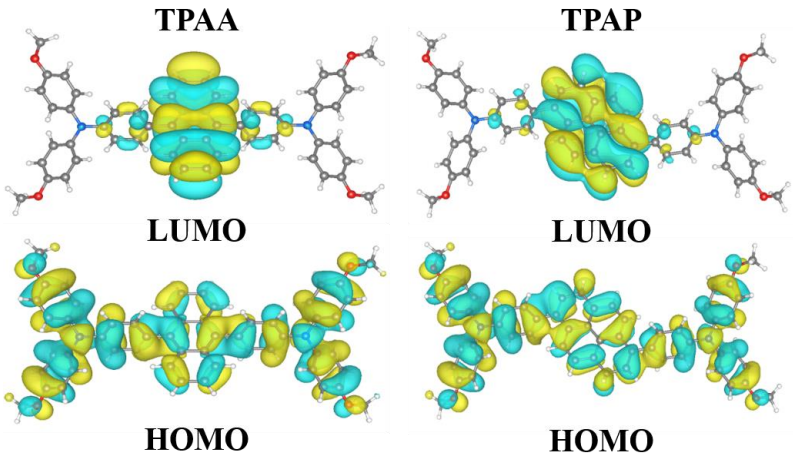

Figure 4.11: HOMO and LUMO plots for TPAA and TPAP based on DFT calculations.

Table 2: HOMO-LUMO energy levels and band-gap (Eg) of PFO,TPAA and TPAP, estimated from density functional simulations and measured from PESA/UV-Vis Absorption.

	DFT			Experimental		
Material	HOMO (eV)	LUMO (eV)	Band gap (eV)	HOMO (eV)	LUMO (eV)	Band gap (eV)
PFO	-5.49	-2.27	3.22	-5.80	-2.10	3.70
TPAA	-5.00	-2.41	2.59	-5.28	-2.68	2.60
TPAP	-4.94	-1.98	2.96	-5.21	-1.86	3.35

As we mentioned already, PFO- which is the high-gap material of our system, already functions as a LED alone. In the case of the PFO:TPAA system, we observe (see Figure 4.12-a) that there is an ideal configuration of the energy levels, since the E_g of TPAA lies completely within the E_g of PFO. Moreover, TPAA can effectively accept energy from the host PFO, through FRET mechanism. Due to higher HOMO level (Figure 4.12-a), it can function as a direct recombination center [98]. This is also supported by the corresponding "tunning" of EL spectra, by varying the dopants composition (see Figure 4.5). We observed that the increase of the guest molecule (TPAA) concentration results in a red shift in the EL spectra.

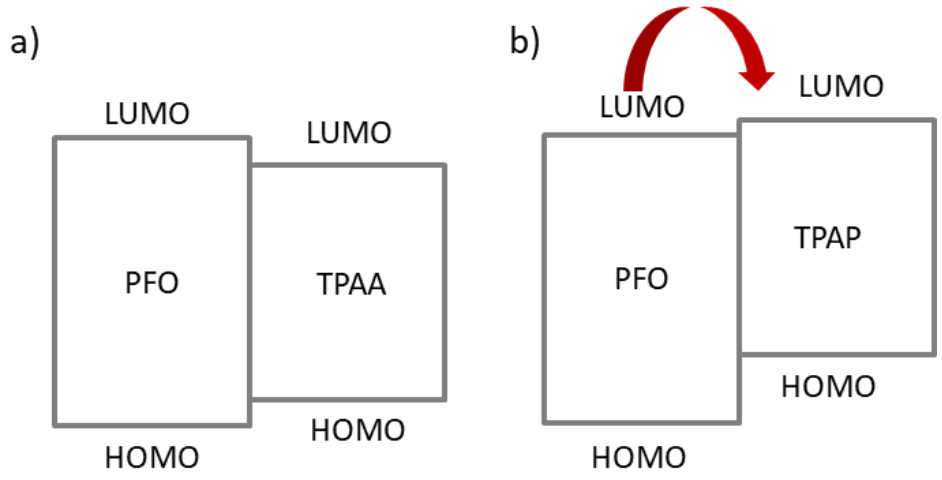

Figure 4.12: Arrangement of energy levels at: a)PFO:TPAA and-b) PFO:TPAP heterojunctions.

However, In the case PFO:TPAP system, we observe that there is a creation of an energy barrier (Figure 4.12-b). The resulting energy barrier provides evidence of charge trapping and explains the lower performance of PFO:TPAP system.

4.7 Time Resolved Photoluminescence Studies

The time resolved photoluminescence (TR-PL) measurements were performed in order to address the excited state lifetime of the respective systems. The PL spectra of both blends exhibit peaks at 463 nm, with an additional shoulder at 500 nm. The peak at 463 nm is assigned to the emission of PFO and the shoulder at 500 nm is attributed to TPAA and TPAP, respectively. The kinetics tracked at the main PL peak at 463 nm are depicted in Figure 4.13 for the respective systems. It is noted, that the neat PFO material exhibits the shortest averaged lifetime, yielding a value of 74 ps. In contrast, the neat TPAA displays substantial longer lifetime of 380 ps and the blended PFO: TPAA system has a lifetime of 96 ps. For the case of the TPAP based blend, the lifetime is estimated to be in the order of 250 ps, whilst the neat TPAP exhibit a lifetime of 407 ps.

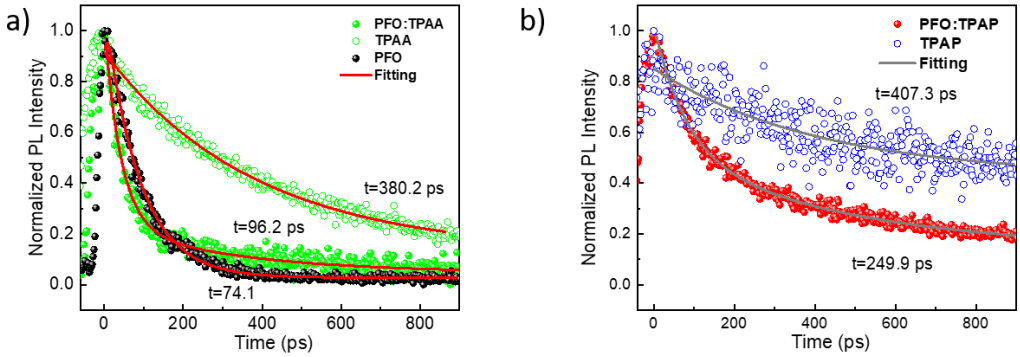

Figure 4.13: TR-PL kinetics of a) neat materials PFO, TPAA and the PFO:TPAA blend upon photoexcitation at 410 nm and- b) TPAP and the PFO:TPAP blend. The solid lines are the associated fits to the experimental data.

The marked difference in the respective blends is due to an enhanced coupling of the excited state with the ground state in the PFO: TPAA system. The shorter lifetime of the neat PFO seems to contribute significantly to the lifetimes of both blends. Fast decay, observed in both systems, is assigned to Förster energy transfer. Overall, fluorescence is more dominant than phosphorescence, leading to significant efficiency limitations.

Chapter 5: Conclusions

We fabricated OLEDs, using conjugated polymer host PFO and two different SMs guests, TPAA and TPAP. Resulted OLED devices combine the solution processing capability of PFO, with the ease of synthesis and batch-to batch reproducibility of SMs. In our case, with the utilization of SM guests, we observed a significant increase in the EQE %. Maximum EQE 2.58 % of our best system (device A) was found to be 6.45 times higher than the maximum EQE % of the PFO only- reference OLED device. It must be noted that we suggest a quite simple device structure, while investigating the ability of our systems, to exhibit EL. Herein we claim two different systems, PFO: TPAA and PFO:TPAP, as a promising emissive layers to achieve an efficient sky-blue OLED.

As the above results indicate, the choice of SM guest is very significant for solution processed OLEDs and can either enhance or decrease the performance of the device. Film morphology studies undoubtedly showed that the control over conformation is important for optimizing performance. We found that TPAA forms more homogenous films compared to TPAP, resulting in more efficient devices.

As a future work, we would like to investigated further the interesting results of the doping effect (see Figure 4.5) and tune OLEDs EL emission from green to deep blue. Moreover, we would like to explore additional or even novel

transporting/injection layers. We believe that this strategy will enable the achievement of higher efficiencies. Ultimately, there are many available pathways through which higher OLED performance can be achieved. Another perspective of future investigation is the effect of ITO surface modification by self-assembled monolayer (SAMs). Recently, it was reported for OPVs studies [99] that the usage of SAMs for modification of ITO anode, increases its working function (WF). Improved charge transfer, efficiency and stability was achieved and this strategy seems promising for the case of OLEDs as well.

OLEDs technology will continue its evolution the next years, providing challenges and inspiration for both academia and research. The upcoming “fourth generation” of OLEDs demands not only novel materials but innovative device architectures as well. Because, at the end of the day, ‘’sky is the limit’’.

APPENDICES

Appendix A: Literature review of device performance. Comparison of PFO:TPAA and PFO:TPAP systems with previous studies on OLEDs.

Emitting layer	EL peak (nm)	Luminance (cd/m^2)	Current efficacy (cd/A)	Turn-on voltage (v)
PFO:TPAA	492	13600	6.65	3.0
PFO:TPAP	497	7000	3.78	3.0
AND:TBP	465	700	3.50	NA
DPF	455	2000	0.6	3.8
OCSoC	455	2700	2.8	4.0
trialkylsilyanthracene	477	107	NA	10

Appendix B: TR-PL

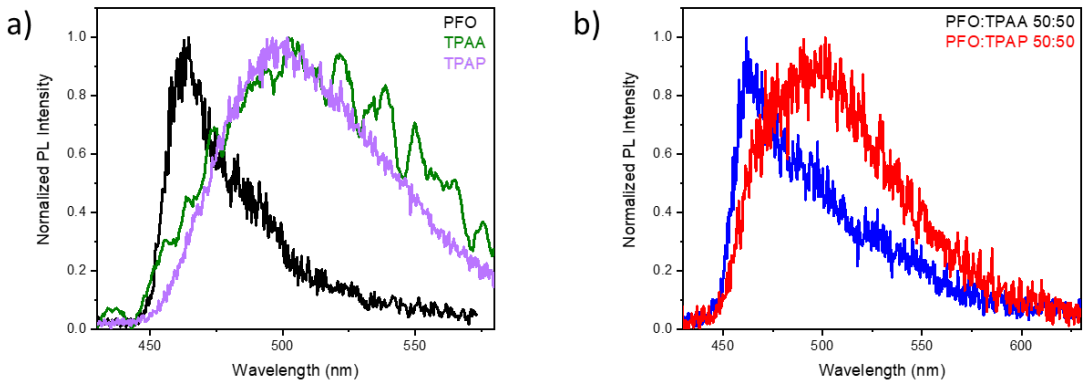

Figure A.C: Time Resolved PL of a) pure PFO, TPAA and TPAP based films – b) of films based on PFO:TPAA (50:50) and PFO:TPAP (50:50) blends.

Appendix C: Host-guest emission-absorption overlap

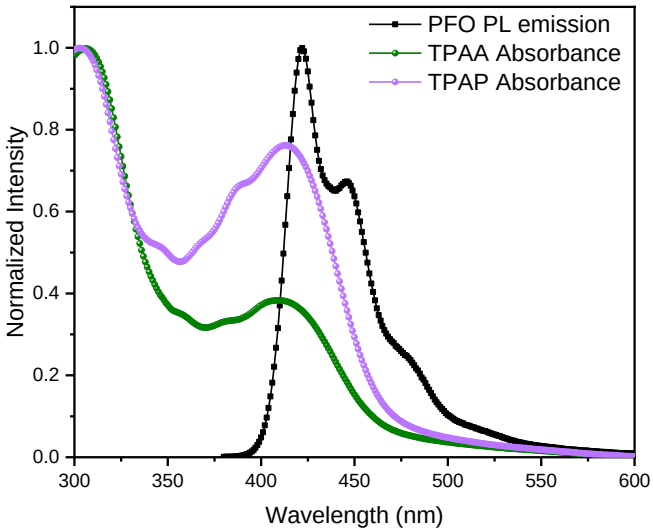

Figure A.C: Overlap between the PL spectrum of PFO host and the absorption spectra of guests TPAA and TPAP.

REFERENCES

[1] O. V Mikhnenko, P. W. M. Blom, and T.-Q. Nguyen, “Exciton diffusion in organic semiconductors,” *Energy Environ. Sci*, vol. 8, p. 1867, 2015, doi: 10.1039/c5ee00925a.

[2] C. Zhang, Y. S. Zhao, and J. Yao, “Organic composite nanomaterials: Energy transfers and tunable luminescent behaviors,” *New J. Chem.*, vol. 35, no. 5, pp. 973–978, May 2011, doi: 10.1039/c1nj20012g.

[3] N. T. Kalyani, H. Swart, and S. J. Dhoble, “Luminescence,” in *Principles and Applications of Organic Light Emitting Diodes (OLEDs)*, Elsevier, 2017, pp. 1–37.

[4] G. Hong *et al.*, “A Brief History of OLEDs—Emitter Development and Industry Milestones,” *Adv. Mater.*, vol. 33, no. 9, p. 2005630, Mar. 2021, doi: 10.1002/adma.202005630.

[5] H. Lei *et al.*, “A solution-processed pillar[5]arene-based small molecule cathode buffer layer for efficient planar perovskite solar cells,” *Nanoscale*, vol. 10, no. 17, pp. 8088–8098, May 2018, doi: 10.1039/c8nr00898a.

[6] “Lab Equipment, Chemicals and Supplies for Materials Science | Ossila.” https://www.ossila.com/ (accessed Apr. 10, 2021).

[7] N. Ohta and A. R. Robertson, *Colorimetry*. Chichester, UK: John Wiley & Sons, Ltd, 2005.

[8] C. W. Tang and S. A. Vanslyke, “Organic electroluminescent diodes,” *Appl. Phys. Lett.*, vol. 51, no. 12, pp. 913–915, Sep. 1987, doi: 10.1063/1.98799.

[9] J. H. Burroughes *et al.*, “Light-emitting diodes based on conjugated polymers,” *Nature*, vol. 347, no. 6293, pp. 539–541, Oct. 1990, doi: 10.1038/347539a0.

[10] Y.-H. Kim, H. Cho, and T.-W. Lee, “Metal halide perovskite light emitters,” *Proc. Natl. Acad. Sci.*, vol. 113, no. 42, pp. 11694–11702, Oct. 2016, doi: 10.1073/PNAS.1607471113.

[11] S. Zou *et al.*, “Stabilizing Cesium Lead Halide Perovskite Lattice through Mn(II) Substitution for Air-Stable Light-Emitting Diodes,” *J. Am. Chem. Soc.*, vol. 139, no. 33, pp. 11443–11450, 2017, doi: 10.1021/jacs.7b04000.

[12] Z. Xu, B. Z. Tang, Y. Wang, and D. Ma, “Recent advances in high performance blue organic light-emitting diodes based on fluorescence emitters,” *Journal of Materials Chemistry C*, vol. 8, no. 8. Royal Society of Chemistry, pp. 2614–2642, Feb. 28, 2020, doi: 10.1039/c9tc06441a.

[13] C. Poriel and J. Rault-Berthelot, “Blue Single-Layer Organic Light-Emitting Diodes Using Fluorescent Materials: A Molecular Design View Point,” *Advanced Functional Materials*, vol. 30, no. 17. Wiley-VCH Verlag, Apr. 01, 2020, doi: 10.1002/adfm.201910040.

[14] S. Nakamura, T. Mukai, and M. Senoh, “High-Power GaN P-N Junction Blue-Light-Emitting Diodes,” *Jpn. J. Appl. Phys.*, vol. 30, no. Part 2, No. 12A, pp. L1998–

L2001, Dec. 1991, doi: 10.1143/JJAP.30.L1998.

[15] D. Wang, C. Cheng, T. Tsuboi, and Q. Zhang, “Degradation Mechanisms in Blue Organic Light-Emitting Diodes,” *CCS Chem.*, vol. 2, no. 4, pp. 1278–1296, Aug. 2020, doi: 10.31635/ccschem.020.202000271.

[16] N. T. Kalyani, H. Swart, and S. J. Dhoble, “Luminescence in Organic Semiconductors,” in *Principles and Applications of Organic Light Emitting Diodes (OLEDs)*, Elsevier, 2017, pp. 39–64.

[17] V. P. Gribkovskii, “Theory of Luminescence,” in *Luminescence of Solids*, Springer US, 1998, pp. 1–43.

[18] T. Tsujimura, *OLED Display Fundamentals and Applications*. Hoboken, New Jersey: John Wiley & Sons, Inc., 2017.

[19] V. K. Khanna, *Fundamentals of solid-state lighting: LEDs, OLEDs, and their applications in illumination and displays*. CRC Press, 2014.

[20] M. Koden, *OLED Displays and Lighting*. Chichester, UK: John Wiley & Sons, Ltd, 2016.

[21] “Mechanism of OLED lighting | What is OLED? | KANEKA CORPORATION KANEKA OLED.” https://www.kanekaoled.jp/en/oled/mechanism.html (accessed Feb. 28, 2021).

[22] Y. Mouhamad, P. Mokarian-Tabari, N. Clarke, R. A. L. Jones, and M. Geoghegan,

"Dynamics of polymer film formation during spin coating," *J. Appl. Phys.*, vol. 116, no. 12, Sep. 2014, doi: 10.1063/1.4896674.

[23] "AR Coating Techniques: Thin Film Deposition Methods." https://www.findlight.net/blog/2017/12/15/ar-coating-techniques/ (accessed Mar. 15, 2021).

[24] S. Coe-Sullivan, "Hybrid Organic/Quantum Dot Thin Film Structures and Devices LIBRARIES Signature of Author," Massachusetts Institute of Technology, 2005.

[25] J. Koskinen, "Cathodic-Arc and Thermal-Evaporation Deposition," in *Comprehensive Materials Processing*, vol. 4, Elsevier Ltd, 2014, pp. 3–55.

[26] Y. K. and C.-S. Ha, *Advances in Organic Light-Emitting Device*. .

[27] J. Shinar, *Organic Light-Emitting Devices*. 2004.

[28] J. Bisquert, G. Garcia-Belmonte, J. M. Montero, and H. J. Bolink, "Charge Injection in Organic Light Emitting Diodes Governed by Interfacial States," 2006.

[29] B. Darade, "Hole-Confining Concept for Blue Organic Light Emitting Diode," 2011.

[30] Seogjoo Jang, *Dynamics of Molecular Excitons*. Elsevier, 2020.

[31] S. R. Forrest, "Excitons and the lifetime of organic semiconductor devices," *Philosophical Transactions of the Royal Society A: Mathematical, Physical and Engineering Sciences*, vol. 373, no. 2044. Royal Society of London, Jun. 28, 2015, doi: 10.1098/rsta.2014.0320.

[32] M. Shukla, N. Brahme, R. S. Kher, and M. Khokhar, “Elementary approach to calculate quantum efficiency of polymer light emitting diodes,” *undefined*, 2011.

[33] X. Ma and H. Tian, “Photochemistry and Photophysics. Concepts, Research, Applications. Von Vincenzo Balzani, Paola Ceroni und Alberto Juris.,” *Angew. Chemie*, vol. 126, no. 34, pp. 8961–8961, Aug. 2014, doi: 10.1002/ange.201405219.

[34] N. J. Turro and V. Ramamurthy, *Modern molecular photochemistry of organic molecules /*. University Science Books, 2010.

[35] B. Patrick O’brien, J. Li, J. Adams, and T. Alford, “New Materials and Device Designs for Organic Light-Emitting Diodes,” 2017.

[36] X. Liang, Z. L. Tu, and Y. X. Zheng, “Thermally Activated Delayed Fluorescence Materials: Towards Realization of High Efficiency through Strategic Small Molecular Design,” *Chemistry - A European Journal*, vol. 25, no. 22. Wiley-VCH Verlag, pp. 5623–5642, Apr. 17, 2019, doi: 10.1002/chem.201805952.

[37] T. J. Penfold, E. Gindensperger, C. Daniel, and C. M. Marian, “Spin-Vibronic Mechanism for Intersystem Crossing,” *Chemical Reviews*, vol. 118, no. 15. American Chemical Society, pp. 6975–7025, Aug. 08, 2018, doi: 10.1021/acs.chemrev.7b00617.

[38] W. A. Luhman and R. J. Holmes, “Investigation of Energy Transfer in Organic Photovoltaic Cells and Impact on Exciton Diffusion Length Measurements,” *Adv.*

Funct. Mater., vol. 21, no. 4, pp. 764–771, Feb. 2011, doi: 10.1002/adfm.201001928.

[39] A. J. Campbell *et al.*, "Origin of electrophosphorescence from a doped polymer light emitting diode," *Phys. Rev. B - Condens. Matter Mater. Phys.*, vol. 63, no. 23, 2001, doi: 10.1103/PhysRevB.63.235206.

[40] D. L. Dexter, "A theory of sensitized luminescence in solids," *J. Chem. Phys.*, vol. 21, no. 5, pp. 836–850, May 1953, doi: 10.1063/1.1699044.

[41] A. Slodek *et al.*, "Highly Luminescence Anthracene Derivatives as Promising Materials for OLED Applications," *European J. Org. Chem.*, vol. 2016, no. 23, pp. 4020–4031, Aug. 2016, doi: 10.1002/ejoc.201600532.

[42] S. Lee *et al.*, "Synthesis and electroluminescence properties of new blue dual-core OLED emitters using bulky side chromophores," *Dye. Pigment.*, vol. 136, pp. 255–261, Jan. 2017, doi: 10.1016/j.dyepig.2016.08.010.

[43] L. Duan *et al.*, "Solution processable small molecules for organic light-emitting diodes," *Journal of Materials Chemistry*, vol. 20, no. 31. Royal Society of Chemistry, pp. 6392–6407, Jul. 27, 2010, doi: 10.1039/b926348a.

[44] S. Zhuang, R. Shangguan, H. Huang, G. Tu, L. Wang, and X. Zhu, "Synthesis, characterization, physical properties, and blue electroluminescent device applications of phenanthroimidazole derivatives containing anthracene or pyrene moiety," *Dye. Pigment.*, vol. 101, pp. 93–102, Feb. 2014, doi:

10.1016/j.dyepig.2013.08.027.

[45] D. Braun, “Semiconducting polymer LEDs,” *Materials Today*, vol. 5, no. 6. Elsevier, pp. 32–39, Jun. 30, 2002, doi: 10.1016/S1369-7021(02)00637-5.

[46] F. Júnior Quites, G. Couto Faria, and T. D. Z. Atvars, “White emission in polymer light-emitting diodes: Color composition by single-layer electroluminescence and external photoluminescence component,” *Mater. Lett.*, vol. 130, pp. 65–67, Sep. 2014, doi: 10.1016/j.matlet.2014.05.079.

[47] X.-Y. Deng, “Light-Emitting Devices with Conjugated Polymers,” *Int. J. Mol. Sci.*, vol. 12, no. 3, pp. 1575–1594, Mar. 2011, doi: 10.3390/ijms12031575.

[48] L. G. T. A. Duarte *et al.*, “The role of a simple and effective salicylidene derivative. Spectral broadening and performance improvement of PFO-based all-solution processed OLEDs,” *Dye. Pigment.*, vol. 171, p. 107671, Dec. 2019, doi: 10.1016/j.dyepig.2019.107671.

[49] K. M. Schelkle *et al.*, “Light-Induced Solubility Modulation of Polyfluorene To Enhance the Performance of OLEDs,” *Angew. Chemie Int. Ed.*, vol. 54, no. 48, pp. 14545–14548, Nov. 2015, doi: 10.1002/anie.201505141.

[50] Y. Nishikitani, H. Takeuchi, H. Nishide, S. Uchida, S. Yazaki, and S. Nishimura, “White polymer light-emitting electrochemical cells using emission from exciplexes with long intermolecular distances formed between polyfluorene and π-conjugated amine molecules,” *J. Appl. Phys.*, vol. 118, no. 22, p. 225501, Dec.

2015, doi: 10.1063/1.4937162.

[51] J. H. Ahn, C. Wang, I. F. Perepichka, M. R. Bryce, and M. C. Petty, “Blue organic light emitting devices with improved colour purity and efficiency through blending of poly(9,9-dioctyl-2,7-fluorene) with an electron transporting material,” *J. Mater. Chem.*, vol. 17, no. 29, pp. 2996–3001, Jul. 2007, doi: 10.1039/b700047b.

[52] C. Wu and J. McNeill, “Swelling-controlled polymer phase and fluorescence properties of polyfluorene nanoparticles,” *Langmuir*, vol. 24, no. 11, pp. 5855–5861, Jun. 2008, doi: 10.1021/la8000762.

[53] M. Ariu, D. G. Lidzey, M. Sims, A. J. Cadby, P. A. Lane, and D. D. C. Bradley, “The effect of morphology on the temperature-dependent photoluminescence quantum efficiency of the conjugated polymer poly(9, 9-dioctylfluorene),” *J. Phys. Condens. Matter*, vol. 14, no. 42, pp. 9975–9986, Oct. 2002, doi: 10.1088/0953-8984/14/42/310.

[54] A. L. T. Khan, P. Sreearunothai, L. M. Herz, M. J. Banach, and A. Köhler, “Morphology-dependent energy transfer within polyfluorene thin films,” *Phys. Rev. B - Condens. Matter Mater. Phys.*, vol. 69, no. 8, p. 085201, Feb. 2004, doi: 10.1103/PhysRevB.69.085201.

[55] B. Al-Asbahi, “Influence of SiO2/TiO2 Nanocomposite on the Optoelectronic Properties of PFO/MEH-PPV-Based OLED Devices,” *Polymers (Basel).*, vol. 10, no.

7, p. 800, Jul. 2018, doi: 10.3390/polym10070800.

[56] A. P. Kulkarni and S. A. Jenekhe, “Blue light-emitting diodes with good spectral stability based on blends of poly(9,9-dioctylfluorene): Interplay between morphology, photophysics, and device performance,” *Macromolecules*, vol. 36, no. 14, pp. 5285–5296, Jul. 2003, doi: 10.1021/ma0344700.

[57] D. Neher, “Polyfluorene Homopolymers: Conjugated Liquid-Crystalline Polymers for Bright Blue Emission and Polarized Electroluminescence,” *Macromol. Rapid Commun.*, vol. 22, no. 17, pp. 1365–1385, Nov. 2001, doi: 10.1002/1521-3927(20011101)22:17<1365::AID-MARC1365>3.0.CO;2-B.

[58] A. Prakash and M. Katiyar, “Correlation between electroluminescence, charge transport and photophysical properties of polymer blends,” *Synth. Met.*, vol. 223, pp. 184–191, Jan. 2017, doi: 10.1016/j.synthmet.2016.11.019.

[59] C. M. Yang, H. H. Liao, S. F. Horng, H. F. Meng, S. R. Tseng, and C. S. Hsu, “Electron mobility and electroluminescence efficiency of blue conjugated polymers,” *Synth. Met.*, vol. 158, no. 1–2, pp. 25–28, Jan. 2008, doi: 10.1016/j.synthmet.2007.11.006.

[60] T. T. Bui, F. Goubard, M. Ibrahim-Ouali, D. Gigmes, and F. Dumur, “Recent advances on organic blue thermally activated delayed fluorescence (TADF) emitters for organic light-emitting diodes (OLEDs),” *Beilstein Journal of Organic Chemistry*, vol. 14, no. 1. Beilstein-Institut Zur Forderung der Chemischen

Wissenschaften, pp. 282–308, Jan. 30, 2018, doi: 10.3762/bjoc.14.18.

[61] "CYNORA Introduces Fluorescent Blue Emitter That Gives OLED Devices a Substantial Efficiency Boost | Business Wire." https://www.businesswire.com/news/home/20200303005067/en/CYNORA-Introduces-Fluorescent-Blue-Emitter-That-Gives-OLED-Devices-a-Substantial-Efficiency-Boost (accessed Mar. 25, 2021).

[62] C. C. Wu, C. I. Wu, J. C. Sturm, and A. Kahn, "Surface modification of indium tin oxide by plasma treatment: An effective method to improve the efficiency, brightness, and reliability of organic light emitting devices ARTICLES YOU MAY BE INTERESTED IN," *Cite as Appl. Phys. Lett*, vol. 70, p. 1348, 1997, doi: 10.1063/1.118575.

[63] Z. Z. You and J. Y. Dong, "Surface properties of treated ITO anodes for organic light-emitting devices," *Appl. Surf. Sci.*, vol. 249, no. 1–4, pp. 271–276, Aug. 2005, doi: 10.1016/j.apsusc.2004.12.006.

[64] R. Po, C. Carbonera, A. Bernardi, F. Tinti, and N. Camaioni, "Polymer- and carbon-based electrodes for polymer solar cells: Toward low-cost, continuous fabrication over large area," *Solar Energy Materials and Solar Cells*, vol. 100. North-Holland, pp. 97–114, May 01, 2012, doi: 10.1016/j.solmat.2011.12.022.

[65] T. M. Goodman, "International standards for colour," in *Colour Design: Theories and Applications: Second Edition*, Elsevier Inc., 2012, pp. 417–452.

[66] S. Nowy, W. Ren, A. Elschner, W. Lövenich, and W. Brütting, “Impedance spectroscopy as a probe for the degradation of organic light-emitting diodes,” *J. Appl. Phys.*, vol. 107, no. 5, p. 054501, Mar. 2010, doi: 10.1063/1.3294642.

[67] P. I. Djurovich, E. I. Mayo, S. R. Forrest, and M. E. Thompson, “Measurement of the lowest unoccupied molecular orbital energies of molecular organic semiconductors,” *Org. Electron.*, vol. 10, pp. 515–520, doi: 10.1016/j.orgel.2008.12.011.

[68] K. Seki and K. Kanai, “Development of Experimental Methods for Determining the Electronic Structure of Organic Materials,” *Mol. Cryst. Liq. Cryst.*, vol. 455, no. 1, pp. 145–181, Oct. 2006, doi: 10.1080/15421400600803713.

[69] G. Haugstad, “Overview of AFM,” in *Atomic Force Microscopy*, Hoboken, NJ, USA: John Wiley & Sons, Inc., 2012, pp. 1–32.

[70] D. Su, “Advanced electron microscopy characterization of nanomaterials for catalysis,” *Green Energy and Environment*, vol. 2, no. 2. KeAi Publishing Communications Ltd., pp. 70–83, Apr. 01, 2017, doi: 10.1016/j.gee.2017.02.001.

[71] P. Wang, C. G. Ebeling, J. Gerton, and R. Menon, “Hyper-spectral imaging in scanning-confocal-fluorescence microscopy using a novel broadband diffractive optic,” *Opt. Commun.*, vol. 324, pp. 73–80, Aug. 2014, doi: 10.1016/j.optcom.2014.03.044.

[72] “Density-Functional Theory of Atoms and Molecules - Robert G. Parr, Yang

Weitao - Oxford University Press." https://global.oup.com/academic/product/density-functional-theory-of-atoms-and-molecules-9780195092769?cc=sa&lang=en& (accessed Mar. 21, 2021).

[73] U. Von Barth, "Basic density-functional theory - An overview," *Phys. Scr. T*, vol. T109, no. T109, pp. 9–39, Jan. 2004, doi: 10.1238/Physica.Topical.109a00009.

[74] M. Valiev *et al.*, "NWChem: A comprehensive and scalable open-source solution for large scale molecular simulations ☆," *Comput. Phys. Commun.*, vol. 181, pp. 1477–1489, 2010, doi: 10.1016/j.cpc.2010.04.018.

[75] A. D. Becke, "Density-functional thermochemistry. III. The role of exact exchange," *J. Chem. Phys.*, vol. 98, no. 7, pp. 5648–5652, Apr. 1993, doi: 10.1063/1.464913.

[76] P. J. Stephens, F. J. Devlin, C. F. Chabalowski, and M. J. Frisch, "Ab Initio calculation of vibrational absorption and circular dichroism spectra using density functional force fields," *J. Phys. Chem.*, vol. 98, no. 45, pp. 11623–11627, 1994, doi: 10.1021/j100096a001.

[77] N. Godbout, D. R. Salahub, J. Andzelm, and E. Wimmer, "Optimization of Gaussian-type basis sets for local spin density functional calculations. Part I. Boron through neon, optimization technique and validation," *Can. J. Chem.*, vol. 70, no. 2, pp. 560–571, Feb. 1992, doi: 10.1139/v92-079.

[78] A. Klamt and G. Schüürmann, "COSMO: A new approach to dielectric screening in

solvents with explicit expressions for the screening energy and its gradient," *J. Chem. Soc. Perkin Trans. 2*, no. 5, pp. 799–805, Jan. 1993, doi: 10.1039/P29930000799.

[79] S. Hirata and M. Head-Gordon, "Time-dependent density functional theory within the Tamm-Dancoff approximation," *Chem. Phys. Lett.*, vol. 314, no. 3–4, pp. 291–299, Dec. 1999, doi: 10.1016/S0009-2614(99)01149-5.

[80] K. Momma and F. Izumi, "VESTA 3 for three-dimensional visualization of crystal, volumetric and morphology data," *J. Appl. Crystallogr.*, vol. 44, no. 6, pp. 1272–1276, Dec. 2011, doi: 10.1107/S0021889811038970.

[81] J. Huang, G. Li, E. Wu, Q. Xu, and Y. Yang, "Achieving high-efficiency polymer white-light-emitting devices," *Advanced Materials*, vol. 18, no. 1. pp. 114–117, Jan. 05, 2006, doi: 10.1002/adma.200501105.

[82] C. C. Chen *et al.*, "Impedance spectroscopy and equivalent circuits of conductively doped organic hole-transport materials," *Org. Electron.*, vol. 11, no. 12, pp. 1901–1908, Dec. 2010, doi: 10.1016/j.orgel.2010.09.005.

[83] P. Chulkin, O. Vybornyi, M. Lapkowski, P. J. Skabara, and P. Data, "Impedance spectroscopy of OLEDs as a tool for estimating mobility and the concentration of charge carriers in transport layers," *J. Mater. Chem. C*, vol. 6, no. 5, pp. 1008–1014, 2018, doi: 10.1039/c7tc04599a.

[84] D. Bozyigit, S. Volk, O. Yarema, and V. Wood, "Quantification of deep traps in

nanocrystal solids, their electronic properties, and their influence on device behavior," *Nano Lett.*, vol. 13, no. 11, pp. 5284–5288, Nov. 2013, doi: 10.1021/nl402803h.

[85] E. Knapp and B. Ruhstaller, "The role of shallow traps in dynamic characterization of organic semiconductor devices," *J. Appl. Phys.*, vol. 112, no. 2, p. 024519, Jul. 2012, doi: 10.1063/1.4739303.

[86] E. Knapp and B. Ruhstaller, "Numerical analysis of steady-state and transient charge transport in organic semiconductor devices," in *Optical and Quantum Electronics*, Oct. 2011, vol. 42, no. 11–13, pp. 667–677, doi: 10.1007/s11082-011-9443-1.

[87] M. Neukom, S. Züfle, S. Jenatsch, and B. Ruhstaller, "Opto-electronic characterization of third-generation solar cells," *Science and Technology of Advanced Materials*, vol. 19, no. 1. Taylor and Francis Ltd., pp. 291–316, Dec. 31, 2018, doi: 10.1080/14686996.2018.1442091.

[88] Y. Di Liu, Q. Zhang, X. H. Yu, J. G. Liu, and Y. C. Han, "Increasing the Content of β Phase of Poly(9,9-dioctylfluorene) by Synergistically Controlling Solution Aggregation and Extending Film-forming Time," *Chinese J. Polym. Sci. (English Ed.*, vol. 37, no. 7, pp. 664–673, Jul. 2019, doi: 10.1007/s10118-019-2259-3.

[89] F. B. Dias, J. Morgado, A. L. Maçanita, F. P. Da Costa, H. D. Burrows, and A. P. Monkman, "Kinetics and thermodynamics of poly(9,9-dioctylfluorene) β-phase

formation in dilute solution," *Macromolecules*, vol. 39, no. 17, pp. 5854–5864, Aug. 2006, doi: 10.1021/ma0602932.

[90] M. N. Yu *et al.*, "Photophysical and Fluorescence Anisotropic Behavior of Polyfluorene β-Conformation Films," *J. Phys. Chem. Lett.*, vol. 9, no. 2, pp. 364–372, Jan. 2018, doi: 10.1021/acs.jpclett.7b03148.

[91] D. F. O'Brien *et al.*, "Electrophosphoresence from a doped polymer light emitting diode," *Synth. Met.*, vol. 116, no. 1–3, pp. 379–383, Jan. 2001, doi: 10.1016/S0379-6779(00)00441-0.

[92] T. Li *et al.*, "Effect of conjugated polymer poly (9,9-dioctylfluorene) (PFO) molecular weight change on the single chains, aggregation and β phase," *Polymer (Guildf).*, vol. 103, pp. 299–306, Oct. 2016, doi: 10.1016/j.polymer.2016.09.072.

[93] J. Peet, E. Brocker, Y. Xu, and G. C. Bazan, "Controlledβ-Phase Formation in Poly(9,9-di-n-octylfluorene) by Processing with Alkyl Additives," *Adv. Mater.*, vol. 20, no. 10, pp. 1882–1885, May 2008, doi: 10.1002/adma.200702515.

[94] T. A. Andersson, K. M. Hartonen, and M. L. Riekkola, "Solubility of acenaphthene, anthracene, and pyrene in water at 50°C to 300°C," *J. Chem. Eng. Data*, vol. 50, no. 4, pp. 1177–1183, Jul. 2005, doi: 10.1021/je0495886.

[95] D. D. C. Bradley *et al.*, "Influence of aggregation on the optical properties of a polyfluorene," in *Optical Probes of Conjugated Polymers*, Dec. 1997, vol. 3145, no. 1, p. 254, doi: 10.1117/12.295530.

[96] M. Grell, D. D. C. Bradley, G. Ungar, J. Hill, and K. S. Whitehead, “Interplay of physical structure and photophysics for a liquid crystalline polyfluorene,” *Macromolecules*, vol. 32, no. 18, pp. 5810–5817, 1999, doi: 10.1021/ma990741o.

[97] A. J. Cadby *et al.*, “Film morphology and photophysics of polyfluorene,” *Phys. Rev. B - Condens. Matter Mater. Phys.*, vol. 62, no. 23, pp. 15604–15609, Dec. 2000, doi: 10.1103/PhysRevB.62.15604.

[98] M. J. Kim, C. W. Lee, and M. S. Gong, “New spirobenzoanthracene derivatives with naphthylanthracene core: Synthesis and application in sky-blue fluorescent host materials,” *Dye. Pigment.*, vol. 105, pp. 202–207, Jun. 2014, doi: 10.1016/j.dyepig.2014.02.005.

[99] Y. Lin *et al.*, “Self-assembled monolayer enables hole transport layer-free organic solar cells with 18% efficiency and improved operational stability,” *ACS Energy Lett.*, vol. 5, no. 9, pp. 2935–2944, Sep. 2020, doi: 10.1021/acsenergylett.0c01421.